



**Effect of Hydrophilicity-Imparting Substituents on Exciton
Delocalization in Squaraine Dye Aggregates Covalently
Templated to DNA Holliday Junctions**

Journal:	<i>Nanoscale</i>
Manuscript ID	NR-ART-09-2023-004499.R1
Article Type:	Paper
Date Submitted by the Author:	20-Nov-2023
Complete List of Authors:	<p>Pascual, Gissela; Boise State University, Micron School of Materials Science & Engineering Roy, Simon; Boise State University, Micron School of Materials Science & Engineering Barcnas , German; Boise State University, Micron School of Materials Science & Engineering Wilson , Christopher; Boise State University, Micron School of Materials Science & Engineering Cervantes-Salguero, Keitel; Boise State University, Micron School of Materials Science & Engineering Obukhova , Olena ; State Scientific Institution "Institute for Single Crystals" of the National Academy of Sciences of Ukraine Krivoshey, Alexander; State Scientific Institution "Institute for Single Crystals" of the National Academy of Sciences of Ukraine Terpetschnig, Ewald; SETA BioMedicals Tatarets, Anatoliy ; State Scientific Institution "Institute for Single Crystals" of the National Academy of Sciences of Ukraine Li, Lan; Boise State University, Micron School of Materials Science & Engineering Yurke, Bernard; Boise State University, Micron School of Materials Science & Engineering; Boise State University, Department of Electrical & Computer Engineering Knowlton, William; Boise State University, Micron School of Materials Science & Engineering; Boise State University, Department of Electrical & Computer Engineering Mass, Olga; Boise State University, Micron School of Materials Science & Engineering Pensack, Ryan; Boise State University, Micron School of Materials Science & Engineering Lee, Jeunghoon; Boise State University, Micron School of Materials Science & Engineering ; Boise State University, Department of Chemistry and Biochemistry,</p>

SCHOLARONE™
Manuscripts

1 Effect of Hydrophilicity-Imparting Substituents on Exciton Delocalization in Squaraine Dye Aggregates

2 Covalently Templated to DNA Holliday Junctions

3 Gissela Pascual, Simon K. Roy, German Barcenas, Christopher K. Wilson, Keitel Cervantes-Salguero,

4 Olena M. Obukhova, Alexander I. Krivoshey, Ewald A. Terpetschnig, Anatoliy L. Tatarets, Lan Li, Bernard

5 Yurke, William B. Knowlton, Olga A. Mass, Ryan D. Pensack, Jeunghoon Lee*

6

7

8

9

10

11 Abstract

12 Molecular aggregates exhibit emergent properties, including the collective sharing of electronic
13 excitation energy known as exciton delocalization, that can be leveraged in applications such as quantum
14 computing, optical information processing, and light harvesting. In a previous study, we found
15 unexpectedly large excitonic interactions (quantified by the excitonic hopping parameter $J_{m,n}$) in DNA-
16 templated aggregates of squaraine (SQ) dyes with hydrophilic-imparting sulfo and butylsulfo substituents.
17 Here, we characterize DNA Holliday junction (DNA-HJ) templated aggregates of an expanded set of SQs
18 and evaluate their optical properties in the context of structural heterogeneity. Specifically, we characterized
19 the orientation of and $J_{m,n}$ between dyes in dimer aggregates of non-chlorinated and chlorinated SQs. Three
20 new chlorinated SQs that feature a varying number of butylsulfo substituents were synthesized and attached
21 to a DNA-HJ via a covalent linker to form adjacent and transverse dimers. Various characteristics of the
22 dye, including its hydrophilicity (in terms of $\log P_{o/w}$) and surface area, and of the substituents, including
23 their local bulkiness and electron withdrawing capacity, were quantified computationally. The orientation
24 of and $J_{m,n}$ between the dyes were estimated using a model based on Kühn-Renger-May theory to fit the
25 absorption and circular dichroism spectra. The results suggested that adjacent dimer aggregates of all the
26 non-chlorinated and of the most hydrophilic chlorinated SQ dyes exhibit heterogeneity; that is, they form a
27 mixture of dimers subpopulation. A key finding of this work is that dyes with a higher hydrophilicity (lower
28 $\log P_{o/w}$) formed dimers with smaller $J_{m,n}$ and large center-to-center dye distance ($R_{m,n}$). Also, the results
29 revealed that the position of the dye in the DNA-HJ template, that is, adjacent or transverse, impacted $J_{m,n}$.
30 Lastly, we found that $J_{m,n}$ between symmetrically substituted dyes was reduced by increasing the local
31 bulkiness of the substituent. This work provides insights into how to maintain strong excitonic coupling
32 and identifies challenges associated with heterogeneity, which will help to improve control of these dye
33 aggregates and move forward their potential application as quantum information systems.

34 Keywords: Hydrophilicity, Frenkel exciton, dye aggregate, soft materials, photophysics, spectrophotometry

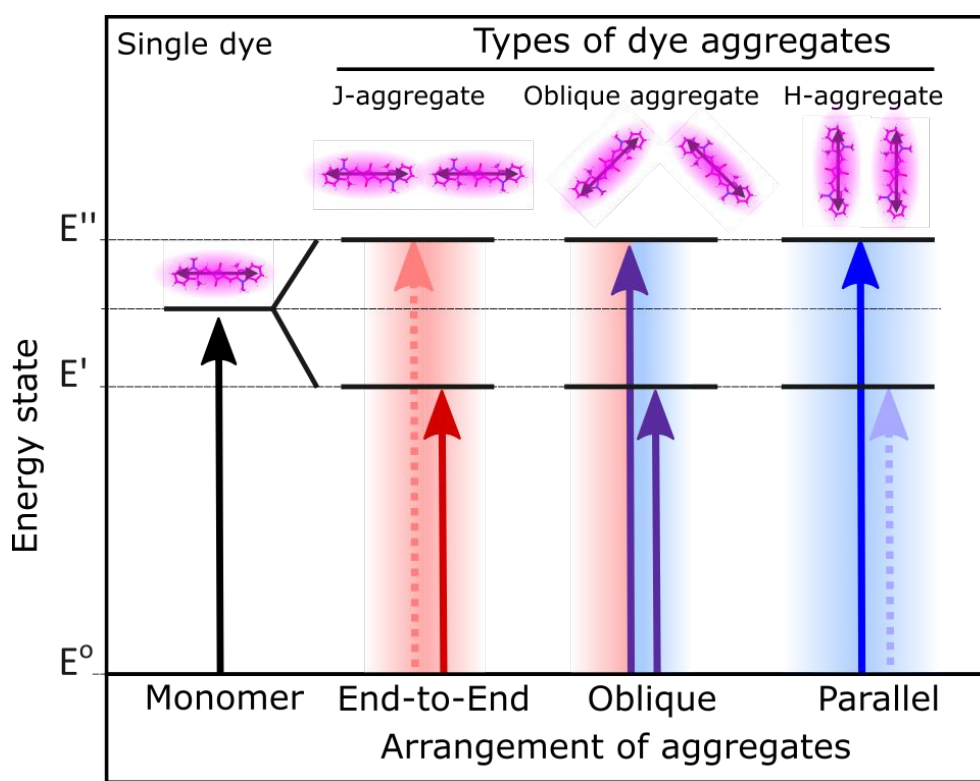
35

36 1. Introduction

37 Molecules (i.e., dyes) can form aggregates through non-covalent interactions, such as electrostatic
38 forces and van der Waals interactions, and exhibit unique optical characteristics due to collective sharing
39 of electronic excitation energy. The collective resonance interaction among excited states of coupled
40 molecules within dye aggregates results in exciton delocalization or Frenkel excitons.¹⁻⁴ Excitons in the
41 photosynthetic machinery, created by the photo-excitation of the molecular aggregates, have inspired
42 extensive research interest in energy conversion, opening new horizons to next-generation technology.
43 Some examples include artificial light-harvesting,^{2,5} nanoscale computing using quantum gates,^{4,6-8} and
44 biological and environmental sensing.^{9,10} In a recent review, Mathur *et al.*¹¹ suggested that quantum
45 computing may be the most extensive impactful application of exciton delocalization, using methodologies
46 provided by Yurke.^{4,8}

47 Based on Frenkel exciton theory, Kasha proposed the excitonic model that describes how exciton
48 interaction depends on the orientation of the transition dipole moment (TDM) vectors of at least two
49 molecules (m and n).¹ These dye molecules contain chromophores that provides them with optically
50 activity. The excitonic hopping parameter ($J_{m,n}$), also known as the excitonic exchange energy or
51 intermolecular Coulombic interaction parameter,¹² measures the strength of excitonic interaction. $J_{m,n}$
52 depends on the orientation of the TDM associated with each molecule within the aggregate. The excitonic
53 coupling model is used to predict the geometry of molecular aggregates based on the resulting exciton states
54 and optical transitions between these states (Figure 1).^{1,13} This model proposes three types of aggregates: J-
55 aggregates, H-aggregates, and oblique aggregates. J-aggregates consist of molecules with TDMs aligned in
56 an end-to-end manner. They display red-shifted (bathochromic) absorption spectra because the only
57 optically allowed electronic transition is from the ground state to the lowest-energy exciton state.
58 Sometimes J-aggregates feature narrow absorption spectral widths, small Stokes shift, and, in principle,
59 shortened excited state lifetimes due to superradiance.¹⁴ H-aggregates consist of molecules with TDMs
60 aligned in a face-to-face manner. They generally exhibit blue-shifted (hypsochromic) absorption spectra

61 because the optically allowed electronic transition is from the ground state to the highest-energy exciton
 62 state. H-aggregates have also been found to exhibit narrow absorption spectral widths¹⁵ and, in contrast to
 63 J-aggregates, the H-aggregates are expected to have longer excited state lifetimes due to subradiance
 64 (although in practice this is rarely found to be the case).¹⁴ Some dyes (*e.g.*, quadrupolar conjugated) might
 65 form H-aggregates that exhibit red-shifted absorption spectra.^{16,17} Oblique aggregates are an intermediate
 66 configuration that are formed by the perpendicular arrangement of TDMs;¹ in this case, optical transitions
 67 from the ground state to both lower and higher energy exciton states are allowed.



68

69 **Figure 1.** The Frenkel molecular exciton model described by Kasha¹ shows the energy transition of dimer
 70 aggregates (J-aggregate, oblique, and H-aggregate) relative to the monomer. A monomer shows the
 71 transition from the ground energy state (E^0) to the first excited energy state. The formation of aggregates
 72 induces exciton delocalization, splitting the excited energy state into higher (E'') and lower (E'). Dashed
 73 arrows indicate the forbidden energy transition. Arrows inside molecules represent the transition dipole
 74 moment (TDM); the TDMs of an oblique dimer is perpendicular.

75

76 The spontaneous aggregation of dyes via non-covalent interaction is sensitive to the characteristics
 77 of the solvent,¹⁸ ionic strength,¹⁹ temperature,²⁰ and polarity²¹. Although many dyes self-assemble in

78 solution under appropriate conditions,^{18–21} the absence of a template makes it difficult to control the
79 geometric arrangement and number of participant dyes in the aggregation. In photosynthetic complexes of
80 plants and bacteria, protein templates enable efficient electronic excitation energy transfer by controlling
81 the geometry of the molecular aggregates and their exciton delocalization. Proteins facilitate the highly
82 compact packing of molecules, known as pigments, enabling strong coupling and energy tuning via
83 molecule-protein interaction.²² Nonetheless, the design of synthetic protein scaffold-based
84 nanoarchitectures for controlling the molecular interaction is still challenging due to many amino acid
85 combinations and complex folding mechanisms. In contrast, sequences of deoxyribonucleic acid (DNA)
86 strands are composed of only four types of bases (adenine, cytosine, guanine, and thymine) which hybridize
87 to form a stable DNA duplex bound by Watson-Crick base pairing between complementary sequences.^{23–}
88 ²⁵ The development of solid-supported synthesis of DNA strands facilitates easy programmability of the
89 base sequences, enabling control over the intermolecular affinity.^{23,26} Current advances in nanotechnology
90 allow the synthesis of branched DNA nanostructures such as four-arm DNA Holliday junctions (DNA-HJ)
91 that are composed of crossover strands with specifically designed base sequences and a fixed branching
92 center.²³ Unique sequences with non-complementary bases in the vicinity of the branch point prevent
93 branch migration, making the DNA-HJ immobile and more stable.²⁵ Dyes can be non-covalently and
94 covalently assembled along the DNA strands. Non-covalent binding allows molecular assembly by
95 intercalating dyes between the nucleobase pairs²⁷ or by binding into the grooves,^{28,29} but the control over
96 position and orientation of the participant dyes in the aggregate is difficult. In contrast, the covalent binding
97 is more advantageous over non-covalent binding due to the robust dye assembly^{26,30} with accurate
98 positioning²⁶ along the DNA strands. Hence, the covalent attachment of dyes to DNA enables the control
99 of the geometry of and $J_{m,n}$ between dyes in dye aggregates, yet these properties can still be influenced by
100 the neighboring nucleobases.³¹

101 During the last decade, squaraine (SQ) and cyanine (Cy) dyes attached to DNA structures have
102 been extensively investigated for their ability to form aggregates and exhibit exciton delocalization.^{12,29,32–}

103 ⁴⁴ SQs and Cys exhibit unique optical properties, such as intense light absorption and fluorescence emission
104 in the visible (VIS) and near-infrared (NIR) spectral regions.^{45–47} Unlike Cys, SQs have an electron-
105 deficient squarate moiety at the center of the pentamethine chain that bridges the electron-rich indolenine
106 rings, which confers a donor-acceptor-donor (D-A-D) structure.^{41,48} The squarate moiety also makes the
107 bridge rigid and planar, suppressing photoisomerization and oxidation compared to dyes with only a
108 polymethine chain; in these respects, this structural modification improves the photostability of SQs
109 compared with Cys. Moreover, SQs are tunable by functionalizing the D and A moieties⁴⁶ with diverse
110 types of substituents for distinct optical and electronic properties. In fact, additional dye properties are
111 impacted by the characteristics of the substituents on the dye periphery.^{28,34,43} Studies demonstrated that
112 dye-dye aggregation relies on the inherent properties of the dyes such as hydrophobicity,^{28,34} steric
113 hindrance (bulkiness of the substituents),⁴³ and the dye position within the template.^{32,34,43}

114 The aggregation of dyes templated by DNA leading to exciton delocalization has been extensively
115 studied.^{12,28–30,32–44,49} A few experimental studies using Cys^{28,43} and SQs³⁴ addressed the influence of dye
116 substituents on the optical properties of DNA-templated molecular aggregates. An earlier study of the
117 hydrophobicity effect on the aggregate formation was conducted by Stadler *et al.*²⁸ using Cy functionalized
118 with methoxy groups or fluorine atoms in which the Cys accumulated into the minor grooves of DNA
119 duplexes. The authors found that dyes symmetrically substituted with methoxy groups promoted stronger
120 aggregate formation than those functionalized with fluorine atoms, but the precise geometry of the
121 aggregates was not reported. Recently, our group investigated the orientation of and $J_{m,n}$ between dyes in
122 dimers and tetramers of a series of six different SQs divided in two sets of hydrophobic and hydrophilic
123 dyes based on their octanol/water partition coefficient ($\log P_{o/w}$).³⁴ The SQ dyes were attached to two
124 complementary or non-complementary strands of the DNA-HJ, via a single flexible 6-carbon linker, to
125 form adjacent or transverse dimers, respectively. The result from hydrophobic dye aggregates confirmed
126 that hydrophobicity promotes their aggregation and exciton delocalization by reducing the center-to-center
127 distance between the dyes and increasing $J_{m,n}$. Larger $J_{m,n}$ was observed for the adjacent dimers as compared

128 with the transverse dimers. Aggregates of the most hydrophobic SQ dye with two chlorine atoms ($SQ-Cl_2$)
129 exhibited the largest $J_{m,n}$ (132 meV)³⁴ as estimated by our in-house KRM Model Simulation tool based on
130 Kühn–Renger–May theory⁵⁰. However, hydrophilic dyes with hydrophilic-imparting substituents sulfo (-
131 Sl) and butylsulfo ($-buSl$) substituents attached to indolenine rings also exhibited aggregation and $J_{m,n}$
132 comparable to hydrophobic dye aggregates. Surprisingly, $SQ-Sl_5$ that has two $-Sl$ and three $-buSl$
133 substituents, which was classified overall as the most hydrophilic via its $\log P_{o/w}$, exhibited a considerably
134 large $J_{m,n}$ (97 meV).³⁴ We suspected that the butyl chains in $-buSl$ substituent increased hydrophobic
135 interactions and promoted the unexpected aggregation of these hydrophilic dyes. Meanwhile, Diaz *et al*⁴³
136 demonstrated that steric hindrance, and to a lesser extent the hydrophobicity, exerts a strong influence on
137 $J_{m,n}$ between symmetrically substituted Cy5s attached to DNA-HJ via 3-carbon linker two-point attachment
138 linkers. In contrast to SQs,³⁴ larger $J_{m,n}$ between Cy5s^{32,43} was reported for transverse dimers potentially due
139 to the different way in which the dyes were attached to the DNA strands.

140 Previous studies provided valuable starting points for understanding the dependence of aggregation
141 and $J_{m,n}$ on dye structure. However, further studies are required to better understand the influence of
142 hydrophilicity and steric effects on $J_{m,n}$ and geometry of dye aggregates. The unexpected aggregation of
143 SQs and their large $J_{m,n}$ by increasing the number of hydrophilic-imparting substituents found in our
144 previous work³⁴ prompted us to investigate an expanded set of SQ dyes. The spatial distribution of
145 substituents around the SQs, either symmetrically or asymmetrically, could play a role in their aggregation
146 propensity or influence their packing geometry. In addition, the position of the SQ-DNA linker could
147 influence the packing and $J_{m,n}$ due to the hydrophobic interaction between the aliphatic linker and the
148 aliphatic chain in a $-buSl$ substituent. The present study introduced three new SQs featuring chlorine atoms
149 ($-Cl$) and $-buSl$ substituents to further our understanding gained from our previous work on the aggregation
150 propensity of SQs, hence $J_{m,n}$.³⁴ This work followed the general hypothesis that hydrophilicity reduces the
151 tendency for molecular aggregation, and hence $J_{m,n}$, because of the reduced SQ-SQ interactions due to
152 higher affinity of such dyes to water. $\log P_{o/w}$ was calculated, along with solvent-accessible surface area

153 (SASA) to gain insights into the characteristics of SQs. The characteristics of substituents, such as their
154 local bulkiness and electron withdrawing capacity, might also play a role in aggregation and $J_{m,n}$. Thus,
155 local bulkiness (A-value) was calculated and their electron withdrawing capacity from literature was used
156 to gain insight into the characteristics of hydrophilic impacting substituent. SQ dimers were templated by
157 DNA-HJ, attaching the SQs to the DNA via a single flexible linker. $J_{m,n}$ between and orientation of the dyes
158 in the dimers were estimated using our KRM model simulation tool; an approach is proposed here to
159 evaluate the presence of single or multiple types of aggregates. In addition, the position of the SQ-DNA
160 linker was changed to investigate the influence of linker position on the $J_{m,n}$ and dye packing.

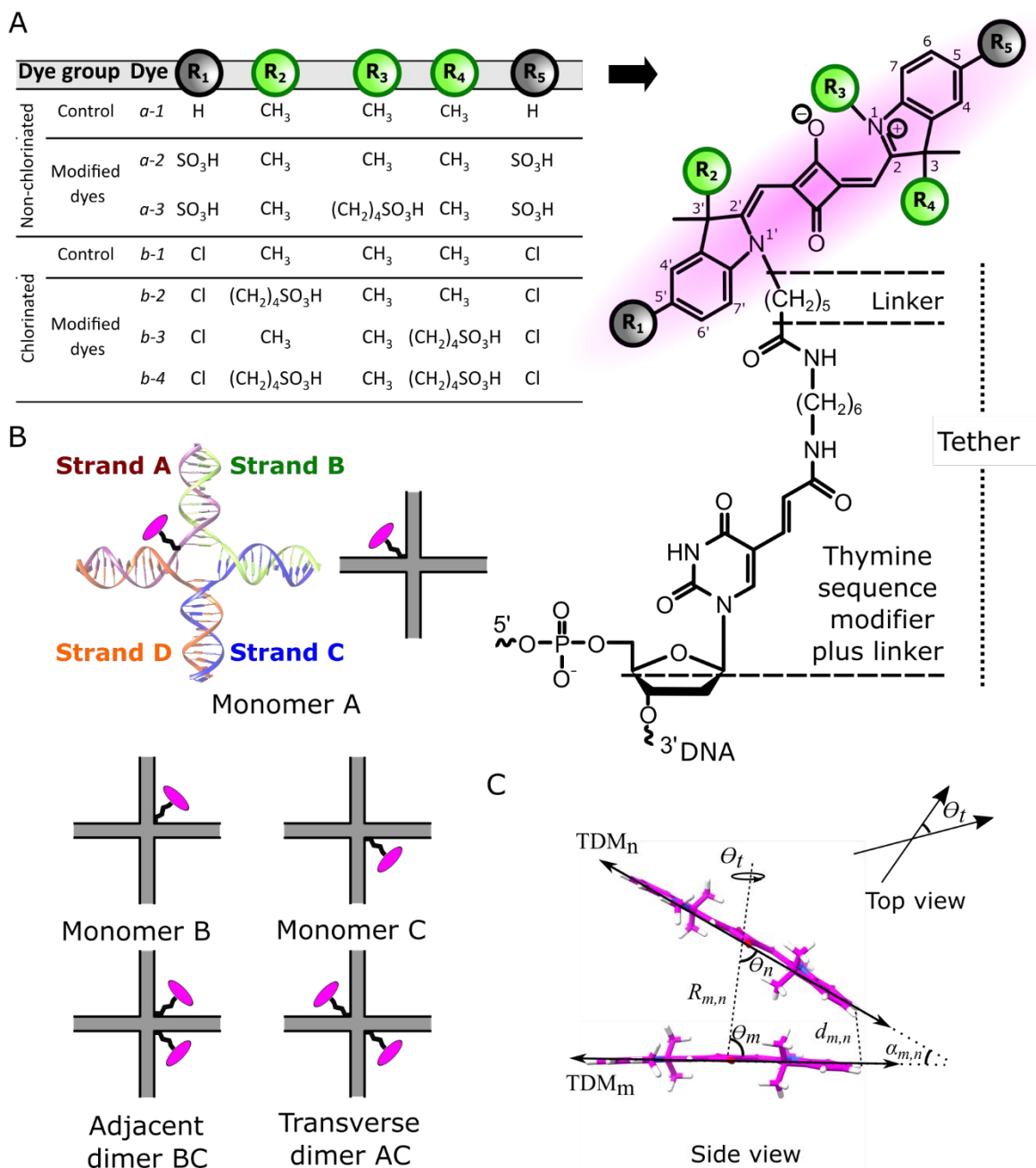
161 2. Material and Methods

162 2.1. Squaraine Dye Synthesis and Preparation of SQ-DNA Constructs

163 The synthesis of the SQs, $SQ-H_2$, $SQ-Sl_2$, $SQ-Sl_3$, and $SQ-Cl_2$ that are hereafter labeled as $a-1$, $a-2$,
164 $a-3$, and $b-1$, respectively, was reported previously.³⁴ $SQ-Sl_5$ of our previous study was not included in the
165 present work due to the presence of a significant amount of optical monomer in the transverse dimer
166 solution at room temperature. These SQs feature hydrophilic-impacting substituents $-Sl$ and $-buSl$. In the
167 present work, the set of dyes was expanded to include three newly synthesized SQs ($b-2$, $b-3$, and $b-4$),
168 which feature $-Cl$ and $-buSl$ substituents (these dyes are hereafter called chlorinated SQs). The synthesis of
169 the new chlorinated SQs that include $-buSl$ substituents is reported in the supplementary information
170 (Section SI 1). The previous finding of our group that aggregates of $b-1$ have the strongest excitonic
171 interactions (highest $J_{m,n}$) among hydrophobic SQs³⁴ prompted the synthesis and further investigation of
172 sulfonated SQ variants such as $b-2$, $b-3$, and $b-4$. Thus, two groups of SQs featuring $-Sl$ and $-buSl$ with their
173 respective controls, were analyzed in the present work (Figure 2A). The first group is non-chlorinated SQs
174 ($a-1$: control, $a-2$, and $a-3$), and the second group is chlorinated SQs ($b-1$: control, $b-2$, $b-3$, and $b-4$).

175 The newly synthesized SQs were covalently attached to the DNA strands, via a single flexible
176 linker, by Integrated DNA Technologies, Inc. and dehydrated until use in downstream experiments. Stock

177 solutions of SQ-DNA at 100 μM were hydrated using ultrapure water (Barnstead Nanopure, Thermo
 178 Scientific). The concentration of SQ-DNA was calculated based on the absorbance at 260 nm measured
 179 using NanoDrop (Thermo Scientific) and the extinction coefficient of the associated DNA absorption band
 180 provided by the supplier.



181
 182 Figure 2. Chemical structure of the non-chlorinated and chlorinated squaraine dyes (SQs) and the
 183 modifications of their functional groups. (A) SQ (with linker and thymine sequence modifier plus linker)
 184 shows the places of the substituents. (B) Schematic representation of SQs monomers and dimers in DNA-

185 HJ. (C) Schematic representation of molecular interaction to understand the geometry of dimers templated
186 by the DNA-HJ (see variables in Table 4).

187 Monomers of *b-2*, *b-3*, and *b-4* and six unique SQ dimers templated by immobile DNA-HJ (Figure
188 2B and Table S1) were prepared using equimolar concentrations (1.5 μM) of four complementary DNA
189 strands (labeled with and without SQs) in $1\times\text{TBE}$, 15 mM MgCl_2 buffer solution. The monomers have one
190 SQ in the strand A, the adjacent dimers have one SQ in two complementary DNA strands (strands B and
191 C), and the transverse dimers have one SQ in two non-complementary DNA strands (strands A and C).
192 Each DNA strand has 26 bases, except the strands labeled with one SQ because they have an additional
193 thymine (14th base position) used to link the SQ via a covalent bond (Figure 2A and Section SI 2). DNA
194 constructs were annealed in an attempt to achieve the homogeneous formation of the target structure.
195 During the annealing process, the samples were heated at 95 $^\circ\text{C}$ (4 min), gradually cooled down until 64
196 $^\circ\text{C}$, and then gradually cooled down to room temperature. Samples were stored at 4 $^\circ\text{C}$ until use in
197 experiments.

198 2.2. Optical Characterization of SQ-DNA Constructs

199 Steady-state absorption of SQ-DNA constructs (monomers and dimer) was recorded at room
200 temperature (22 $^\circ\text{C}$) using a UV-Vis-NIR absorption spectrophotometer (Agilent, Cary 5000) in dual-beam
201 mode. The SQ-DNA construct solution (1.5 μM) was contained in a 50 μL capacity quartz cuvette of 1 cm
202 path length. Absorption spectra were recorded twice from 230 to 800 nm wavelength in 1 nm steps.

203 Circular dichroism (CD) of the SQ-DNA constructs was measured using a spectropolarimeter (J-
204 1500, JASCO). The solution of SQ-DNA construct (1.5 μM) was contained in a 100 μL capacity quartz
205 cuvette (Starna cells) of 1 cm path length. CD spectra were recorded from 230 to 800 nm three times at 200
206 nm/min.

207 Steady-state fluorescence spectra were recorded using a fluorescence spectrometer (Fluorolog-3,
208 Horiba Scientific) with the sampled contained in a 1 cm path-length quartz cuvette (Starna cells). Details
209 of additional experimental parameters, such as excitation wavelength, are reported where appropriate.

210 2.3. Characterization of Squaraine Dyes and Their Substituents

211 SQs were characterized by theoretically calculating the octanol/water partition coefficient ($\log P_{o/w}$)
212 which we use as a general proxy for the overall hydrophilicity of the SQ, and the solvent accessible surface
213 area (SASA). In this work, $\log P_{o/w}$ was calculated following the approach described by Garrido *et al.*,⁵¹
214 which is the same approach used for non-chlorinated dyes and the *b-1* SQ.³⁴ $\log P_{o/w}$ was calculated based
215 on the absolute solvation Gibbs energies⁵¹ using the Gaussian software package⁵² following eq. 1. It is the
216 negative value of the difference of solvation energies between *n*-octanol (ΔG_o) and water (ΔG_w) calculated
217 using density functional theory (DFT)⁵³ divided by 2.3 times the gas constant ($R = 8.31 \text{ J/mol}\cdot\text{K}$) and
218 temperature ($T = 273.15 \text{ K}$). More negative and more positive $\log P_{o/w}$ values indicate more hydrophilic
219 and hydrophobic behavior of SQs, respectively.

$$220 \quad \log P_{o/w} = -\frac{\Delta G_o - \Delta G_w}{2.303RT} \quad (\text{eq. 1})$$

221 The molecular geometry of SQ was initially approximated using the force fields model (UFF)⁵⁴
222 using Avogadro⁵⁵ open license software. Then, structures were optimized using Gaussian 16 software
223 package with the 6-31+G (d,p) basis set with the M06-2X exchange correlation functional.⁵⁶

224 The optimized SQ structures in water were used to calculate the SASA for the entire dye. SASA
225 was calculated by using the optimized ground state structure inside of the ChimeraX⁵⁷ software package
226 and using the measured SASA function. Increased SASA (\AA^2) indicates a larger dye surface area that is
227 accessible by the solvent (water), but this increased SASA does not necessarily indicate a higher affinity to
228 water. The affinity to water of a dye is assessed using $\log P_{o/w}$. The SASA and hydrophilicity are
229 characteristics of SQs described by the number of substituents and their identity such as chlorine atoms (-
230 *Cl*) and sulfonic acid (sulfo) $-SO_3H$ (*-Sl*) and butylsulfo $-(CH_2)_4SO_3H$ (*-buSl*) groups.

231 The local bulkiness or steric hindrance of substituents of SQ was quantified by the A-value, which
232 measures the difference in energy between the equatorial and axial conformation of cyclohexane in the
233 presence of the substituent. A high A-value of SQs generated using the Gaussian software package⁵²

234 characterizes locally bulkier substituents. The free energy of each SQ was taken from the thermochemical
235 data produced during the frequency calculation of each SQ without solvent. The output was analyzed with
236 the cclib Python library.⁵⁸

237 2.4. KRM Modeling and Data Analysis

238 The orientation of and $J_{m,n}$ between dyes in SQ aggregates were calculated using the in-house-
239 developed KRM model simulation tool (version ev13v5, 2022). The KRM modeling tool simultaneously
240 fits absorbance and CD spectra to estimate orientation of and $J_{m,n}$ between dyes in the aggregate (Figure
241 2C). Absorption and CD spectra data of SQ-DNA constructs in solution were collected at room temperature
242 to prevent an influence of temperature²⁰ on the dye aggregation. In previous studies, the KRM model
243 simulation tool has been successfully applied to calculate the geometry of and $J_{m,n}$ between dyes in dye
244 aggregates.^{12,32–34,43} The theoretical formulation⁵⁰ for the KRM model was described in detail by Roy *et al.*³³
245 Briefly, the KRM model uses the TDM vector length (1.3 nm) and absorption spectrum (in extinction
246 coefficient), to find the fitting parameters of a monomer such as the energy a vibron (eV), the displacement
247 of the excited state potential from the ground state potential (d), and the energy loss parameter (I). These
248 parameters allow the tool to calculate the TDM amplitude of the monomer in units of debye (D) along with
249 the characteristic exciton hopping parameter (J_0) in units in millielectronvolts (meV). J_0 is a constant pre-
250 factor for calculation of $J_{m,n}$.³³ CD of monomers is not needed because only aggregates are expected to
251 exhibit CD signal. However, the CD of monomers is not necessarily zero as shown for SQs³⁴ but essentially
252 is negligible.⁵⁹ Using the features of the monomers and offset energy of dimers (E_{of}), allows the calculation
253 of $J_{m,n}$ between dyes and the dye aggregate packing geometry by simultaneously modeling their absorption
254 and CD spectra. The KRM modeling tool calculates the shortest distance ($d_{m,n}$) between the two TDM
255 vectors of the dyes (approach of single dimer) using a limited distance of 0.34 nm. This minimum distance
256 was chosen based on the minimum distance between SQs (0.35 nm) in single crystals of indolenine-based
257 selenium-substituted SQs.⁶⁰

258 In this study, single (homogeneous) versus multiple (heterogeneous) populations of aggregate
259 structures in solution were examined using a new KRM modeling approach. First, the optical properties are
260 modeled using a single population of aggregates, which uses two TDM vectors, one for each dye in the
261 dimer. If the result shows that the normalized overlap integral of the experimental and theoretical absorption
262 and CD spectra are high (*e.g.*, $\geq 90\%$), the dimer is assigned as a single type of dimer population. However,
263 if the normalized overlap integral of the experimental and theoretical absorption and CD spectra are low
264 (*e.g.*, $\leq 90\%$), an intensive KRM modeling was performed following a new approach that accounts for a
265 heterogeneous population of aggregate types. The new approach uses four TDM vectors for two dimer
266 populations. The distance between dimers was set to 1 μm to ensure that $J_{m,n}$ between dyes in the separated
267 dimers is effectively zero. This distance is reasonably expected for dye aggregates sufficiently separated
268 from each other due to the size of the DNA-HJ and the electrostatic repulsion imposed by the DNA
269 duplexes. The best fit between the two modeling approaches was determined based on the higher value of
270 normalized overlap integral of both experimental and theoretical data. A significant fitting improvement
271 was observed for adjacent dimers *a-1*, *a-2*, and *a-3* when using the heterogeneous population approach as
272 compared with the previously used single type of dimers approach.³⁴

273 The relationship between the maximum $J_{m,n}$ and dye properties (*e.g.*, water affinity) was evaluated
274 using linear regression analysis, in which the coefficient of determination R-square (R^2) is scaled from 0 to
275 1. This coefficient represents the proportion of variation in $J_{m,n}$ that can be explained by the properties of
276 SQs.

277 3. Results and Discussion

278 3.1. Structural Characteristics and Physical Properties of Squaraine Dyes (SQs)

279 The present work used chlorinated and non-chlorinated sets of SQs with their respective controls
280 *a-1* and *b-1* (Figure 2A). The physical properties of SQs, such as ΔG_w and ΔG_o , $\log P_{o/w}$, and SASA, rely
281 on the structural characteristics of the substituents (Table 1). The structural characteristics and physical

282 properties of the non-chlorinated SQs (*a-1*, *a-2*, and *a-3*) and the chlorinated SQ *b-1* were described in our
 283 previous study.³⁴ Here, we first briefly compared the properties between *a-1* and *b-1*. Then, we compared
 284 the SQs, that featured hydrophilic-imparting substituents, with their respective controls to give context of
 285 KRM modeling in Section 3.4.

286 The control dyes *a-1* and *b-1* have *H* and *Cl* atoms, respectively, at positions 5- and 5'- in the
 287 indolenine rings. Compared to *a-1* ($\Delta G_w = -79$, $\Delta G_o = -102$ kJ/mol), *b-1* exhibits a reduced solvation energy
 288 in water and octanol ($\Delta G_w = -82$, $\Delta G_o = -110$ kJ/mol). Changes in the ΔG resulted in a higher log $P_{o/w}$ for
 289 *b-1* (5.31) as compared with *a-1* (4.30), revealing that *b-1* had less affinity to water (less hydrophilic) than
 290 *a-1*. The less hydrophilic behavior of *b-1* arises from the chlorine atoms that also increase the SASA from
 291 665 Å² (*a-1*) to 740 Å² (*b-1*), reflecting the larger atomic size of chlorine compared with hydrogen.

292

293 Table 1. Characteristic of squaraine dyes (SQs) using theoretical approaches

Dye Group	Dye	^a ΔG_w [kJ/mol]	^b ΔG_o [kJ/mol]	^c Log $P_{o/w}$	^d SASA [Å ²]	
Non-chlorinated ^d	Control	<i>a-1</i>	-79	-102	4.30	665
	Modified dyes	<i>a-2</i>	-181	-161	-3.66	825
		<i>a-3</i>	-244	-211	-6.26	920
Chlorinated	Control ^d	<i>b-1</i>	-82	-110	5.31	740
	Modified dyes	<i>b-2</i>	-92	-104	2.18	849
		<i>b-3</i>	-92	-104	2.18	849
		<i>b-4</i>	-205	-203	-0.38	999

^a ΔG_w in kJ/mol, is the solvation energy in water.

^b ΔG_o in kJ/mol, is the solvation energy in *n*-octanol.

^cLog $P_{o/w}$ calculated without linker. The linker imparts similar effect to the studied dyes (variation of log $P_{o/w}$ by including the linker: 1.96 - 2.59)³⁴

^dThe solvent (water) accessible surface area (SASA) of the entire dye is given in Angstroms square (Å²).

^{a,b,c}Values of non-chlorinated and *b-1* were calculated in our previous study.³⁴

294

295 Non-chlorinated SQs *a-2* and *a-3* have *-Sl* at positions 5- and 5'- in the indolenine rings as
 296 compared with *a-1* (Figure 2A). Additionally, *a-3* has a *-buSl* group at position 1 in the indolenine ring.
 297 Compared with *a-1*, lower log $P_{o/w}$ values were obtained for *a-2* and *a-3*. The presence of two *-Sl* groups in

298 *a-2* as compared with two hydrogen atoms in *a-1* caused ΔG_w to decrease from -79 to -181 kJ/mol and ΔG_o
299 to decrease from -102 to -161 kJ/mol. Likewise, the $\log P_{o/w}$ was reduced from 4.30 to -3.66. The larger
300 SASA of *a-2* (825 Å²) than *a-1* (665 Å²) reflects the larger structural size of *-Sl* than *-H*. The additional
301 presence of the *-buSl* group in *a-3* further reduced both ΔG_w and ΔG_o (Table 1). Thus, *a-3* resulted in the
302 most hydrophilic dye among SQs in this study ($\log P_{o/w} = -6.26$). *a-3* also had the largest SASA (920 Å²)
303 among the non-chlorinated SQs.

304 The chlorinated SQs *b-2* and *b-3* have *-buSl* at position 3' and 3 in the indolenine rings,
305 respectively, as compared with *b-1* (Figure 2A). *b-2* and *b-3* have similar optical properties but their
306 chemical structures are different because the position of the substituent change with respect to the position
307 of the SQ-DNA linker. Specifically, the SQ-DNA linker and the *-buSl* substituent are located on the same
308 indolenine ring in *b-2*, whereas the SQ-DNA linker and the *-buSl* substituent are located on different
309 indolenine rings in *b-3* (Figure 2A). The relative position of the *-buSl* substituent and SQ-DNA linker was
310 purposely changed to investigate its influence on $J_{m,n}$. The *-buSl* substituent in *b-2* and *b-3* reduced the ΔG_w
311 to -92 kJ/mol as compared with ΔG_w of *b-1* of -82 kJ/mol. The presence of *-buSl* in *b-2* and *b-3* also slightly
312 increased ΔG_o to -104 kJ/mol as compared with ΔG_o of *b-1* of -110 kJ/mol. The slightly increased ΔG_o
313 likely is due to the presence of the hydrophobic butyl chain in the *-buSl* substituent. Additionally, the \log
314 $P_{o/w}$ was reduced from 5.31 in *b-1* to 2.18 in *b-2* and *b-3*, indicating an increased affinity to water of these
315 two SQs. The larger SASA of *b-2* and *b-3* (849 Å²) than *b-1* (740 Å²) reflects the larger structural size of *-*
316 *buSl* than *-Cl*. The symmetrically substituted *b-4* has *-buSl* in positions 3- and 3' of the indolenine ring. *b-*
317 *4* exhibited nearly two times the ΔG_w and ΔG_o of *b-1*, *b-2*, and *b-3*; the presence of a sulfonate group and a
318 butyl chain in the *-buSl* substituent increased the ΔG_w and ΔG_o , respectively. The $\log P_{o/w}$ of *b-4* became
319 slightly negative (-0.38) and SASA increased due to the presence of two *-buSl* substituents. Compared to
320 the other chlorinated SQs, the close to zero value for the $\log P_{o/w}$ of *b-4* suggests its affinity to both polar
321 and non-polar solvents due to presence of *-buSl* substituents. The presence of a *-buSl* substituent in *b-2* and

322 *b-3* may also confer affinity to polar and non-polar solvents to these dyes, but with a smaller propensity as
 323 compared to *b-4*.

324 Finally, the presence of *-Sl* and *-buSl* substituents in the non-chlorinated dyes resulted in a larger
 325 reduction of log $P_{o/w}$ as compared with the introduction of only *-buSl* substituents in the chlorinated SQs.
 326 These results indicate that *-Cl* enhanced the hydrophobic behavior of SQs and that the *-buSl* substituent
 327 imparted less hydrophilicity as compared with the *-Sl* group.

328 3.2. Characteristics Squaraine Dyes (SQs) Substituents

329 The Hammett constant (σ) and A-value were used to compare the effect of substituent on electronic
 330 and steric effects, respectively. The electronic effect⁶¹ described by σ relies on the inductive and resonance
 331 effects of the substituent in the benzene ring. The packing of SQs might rely on σ that represents the
 332 electronic effect of replacing *-H* with *-Cl* and *-Sl* on the aromatic rings. Substituents with a high electron-
 333 withdrawing capacity compared to *-H* ($\sigma = 0$) show positive σ values, while substituents having a high
 334 electron-donating capacity show negative values. For the present study, para position (σ_p) is pertinent
 335 because indolenine rings of SQs are substituted in position para, e.g., from 4-chlorophenylhydrazine (SI 1).
 336 According to σ_p , the substituents used in the present study are characterized by their moderate (*-Sl*) and
 337 weak (*-Cl*) electron-withdrawing capacity (Table 2).

338 Table 2. Characteristics of substituents of squaraine dyes (SQs)

Name	Chemical formula	Representation	A-value ^a [kcal/mol]	σ_p ^b
Hydrogen	H	<i>-H</i>	0	0
Chlorine	Cl	<i>-Cl</i>	0.47	0.23
Butylsulfo	(CH ₂) ₄ SO ₃ H	<i>-buSl</i>	1.83	n/a
Sulfo	SO ₃ H	<i>-Sl</i>	2.25	0.35

^aCalculated using DFT.

^bHammett constant in position para (σ_p) was calculated by Hansch *et al.*⁶¹
 Hammett constant (σ) of SO₃⁻ was used as a reference of SO₃H.

n/a: σ for dyes *b-2* and *b-3* are not applicable because *-buSl* substituents are not conjugated with the indolenine rings of the SQs.

339 The local bulkiness of the substituents is characterized by high A-value that quantifies the
340 difference of conformational energy when the substituent is in the equatorial or axial position on
341 cyclohexane. A previous study⁴³ found that the local bulkiness can be helpful in understanding trends in
342 molecular packing. The DFT-calculated A-values of *-Cl* (0.47 kcal/mol), *-buSl* (1.83 kcal/mol), and *-Sl*
343 (2.25 kcal/mol) showed that local bulkiness better reflects the spatial arrangement of the atoms on the
344 substituents rather than the overall size of the substituent (Table 2). These results were compared with the
345 control *-H* (A-value = 0). The A-value of *-Cl* calculated in the present study was close to a value previously
346 reported in monosubstituted cyclohexane conformer, 0.51 kcal/mol.⁶² Comparison of the A-value of *-buSl*
347 in the present study was limited to the closest structure available in the literature of ethyl chain (A-value
348 1.79 kcal/mol).⁶³ The higher A-value of *-buSl* compared to the A-value of the ethyl chain in the literature⁶³
349 is ascribed to the presence of the additional ethylene and sulfo moieties.

350 Comparison of the influences of substituent properties (σ and A-value) on the dye properties (log
351 $P_{o/w}$ and SASA) were made using only symmetrically substituted *a-1*, *a-2*, and *b-1*, which have one
352 substituent in each indolenine ring. Compared with *-Sl*, *-Cl* has a lower electron withdrawing capacity and
353 it is less bulky. In regard to the properties of SQs, the hydrophilicity increased in the order *b-1* < *a-1* <<
354 *a-2*, while SASA increases in the order *a-1* < *b-1* < *a-2*. Although the large molecular size of substituents
355 increased SASA, it did not necessarily enhance the hydrophilicity of SQs because the latter depends on the
356 presence of polar groups rather than molecular size. By coincidence, the A-value and SASA follow similar
357 tendencies (Table 2); while A-value represents the energetic preference imparted by the substituents on
358 cyclohexane for the equatorial position, SASA represents the physical size of a SQ.

359 3.3. Photophysical Properties and Exciton Delocalization of SQ-DNA constructs

360 The optical characteristics of monomers and dimers of non-chlorinated and chlorinated SQs are
361 briefly summarized to give a context to the KRM modeling results in Section 3.4. Extended information
362 regarding the steady-state optical characterization of monomers and aggregates of non-chlorinated SQs and
363 *b-1* dye is reported in our previous study.³⁴ The propensity for aggregation of SQ dyes was confirmed by

364 changes in their optical properties such as absorption and fluorescence spectra (Table 3 and Figures 3 and
 365 4). The SQ monomers attached to DNA-HJ showed absorption peaks between 638 and 649 nm, which are
 366 consistent with the main absorption peak of modified SQ dyes reported in previous studies^{47,64} (Table 3 and
 367 Section SI 3). The *b-1* monomer exhibited a peak at 645 nm which is red-shifted relative to the peak at 638
 368 nm in the unmodified *a-1* monomer. The presence of an electron-withdrawing *-Cl* substituent in *b-1* (Table
 369 3) results in a red-shifted absorption spectrum.

370

371 Table 3. Optical properties of squaraine dyes (SQs) monomers and dimer

Dye Group	SQ dye	Monomer	Adjacent Dimer			Transverse Dimer			
		Maximum peak (nm)	Maximum peaks (nm)	A2/A1 ^a	FS ^b [%]	Maximum peaks (nm)	A2/A1 ^a	FS ^b [%]	
Non-Chlorinated	Control	<i>a-1</i>	638	592; 629	1.3	91	606; 632	0.8	87
	Modified dyes	<i>a-2</i>	640	598; 630	1.2	85	607; 630	1.2	90
		<i>a-3</i>	636	594; 631	1.3	69	596; 632	0.8	77
Chlorinated	Control	<i>b-1</i>	645	596; 633	3.7	93	600; 633	2.0	94
	Modified dyes	<i>b-2</i>	647	598; 632	3.3	72	601; 641	0.9	87
		<i>b-3</i>	647	599; 636	2.6	46	604; 641	0.6	73
		<i>b-4</i>	649	603;638;655	^c	73	603; 643	0.6	76

Experiments were conducted at 1x TBE buffer, 15 mM MgCl₂ containing 1.5 μM DNA construct at room temperature (22 °C). Data of non-chlorinated and *b-1* dyes were calculated from absorption and fluorescence data presented in our previous study.³⁴

^aA2/A1: Is the ratio of absorbance peak at high energy (low wavelength) / absorbance peak at low energy (high wavelength) of experimental data (Figures 3 and 4).

^bThe fluorescence emission was scaled with absorbance to calculate the fluorescence suppression (FL) of dimer in reference to their monomers.

^cThis structure showed three peaks (Figure 3)

372

373 Compared with the 638 nm absorption maximum of the *a-1* monomer control, non-chlorinated *a-2*
 374 exhibited a slightly red-shifted absorption peak at 640 nm and *a-3* showed a blue-shifted peak at 636 nm.³³
 375 Compared with the 645 nm absorption maximum of the *b-1* monomer control, chlorinated SQs *b-2*, *b-3*,
 376 and *b-4* exhibited slightly red-shifted peaks at 647, 647, and 649 nm, respectively. The red-shifted effect
 377 upon the addition of *-buSl* substituents was also reported for free dyes;⁴⁷ that is, the dyes not tethered to

378 DNA. Furthermore, it seems that the optical properties of chlorinated SQs are influenced by the electron-
379 withdrawing ability of chlorine atoms, which may also potentially influence their aggregation propensity
380 and $J_{m,n}$. This red-shift effect of $-Cl$ substituent was also reported in previous studies of Cy5s⁴³ and SQs.³⁴

381 All dimers exhibited a blue-shifted absorption peak relative to the lowest-energy monomer peak,
382 which is a characteristic of H-aggregates.¹ The adjacent $b-4$ dimer also exhibited a red-shifted absorption
383 peak. Moreover, the amplitude of the absorption peak at high energy (noted as A2) was usually greater than
384 the absorption peak at low energy (noted as A1), the latter of which aligns with the absorption maximum
385 of the corresponding monomer (Figures 3 and 4). The A2/A1 ratio determined from the absorption spectra,
386 which can be used to gauge aggregation propensity or excitonic coupling assuming a single aggregation
387 (H-aggregation), was higher in adjacent dimers (1.2 – 3.7) than in transverse dimers (0.6 – 2.0). These
388 results indicate either stronger propensity for aggregation or stronger excitonic coupling in the adjacent
389 dimers (Table 3). The generally lower A2/A1 ratio of the chlorinated dyes (0.6 – 0.9), of transverse dimers,
390 is indicative of either a weaker propensity for aggregation or a weaker excitonic coupling. There is a
391 noticeable effect on the absorption spectra of the adjacent dimers by changing the relative position of the -
392 $buSl$ substituent and SQ-DNA linker in the case of $b-2$ and $b-3$. The A2/A1 ratio is higher when the $-buSl$
393 substituent and the SQ-DNA linker are attached to the same indolenine ring (A2/A1 of $b-2 = 3.3$) compared
394 to when they are attached to rings on opposite sides (A2/A1 of $b-3 = 2.6$). $b-4$ dimer showed three absorption
395 peaks, which suggests a potential mixture of ensemble-level subpopulations with different dye packing
396 arrangement (*e.g.*, H- and J-aggregates) that was further examined using the KRM modeling tool. We
397 attribute the bands at 603 and 638 nm to H-aggregates and the band at 655 nm to J- aggregates (Figure 4).

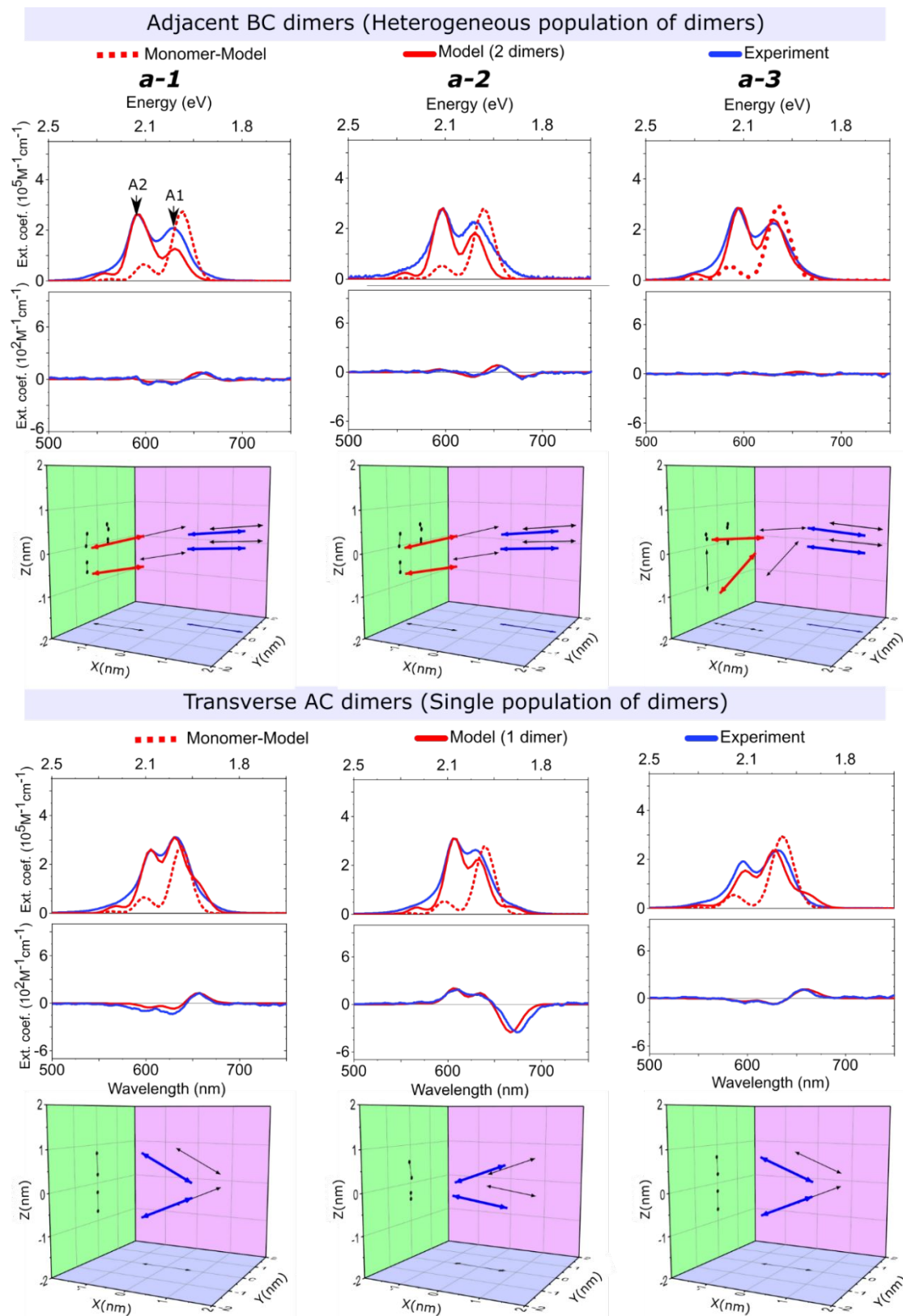
398 Adjacent dimers showed lower CD intensity compared to transverse dimers (Figure 3 and 4). The
399 difference of the SQ-DNA linker positions between $b-2$ and $b-3$ reduced the CD spectra intensity of these
400 dimers and shifted the signature from negative to positive signal. The CD signal of aggregates relies on $J_{m,n}$,
401 which is governed by the proximity and mutual orientation of TDMs.³³ A strong CD signal indicates
402 excitonic interactions, whereas a weak signal does not necessarily preclude these interactions. A weak CD

403 signal could also indicate that the ensemble-level sample consists of a heterogeneous mixture of dimer
404 subpopulations with different packing configurations.³³ In fact, the formation of two aggregate
405 subpopulations in the adjacent dimers of non-chlorinated SQs with different packing arrangements is
406 supported by KRM modeling (Section 3.4). The high intensity of the bisignate CD spectra of *b-2*, *b-3*, and
407 *b-4* transverse dimers compared to the *b-1* transverse dimer indicates that the TDMs were twisted, which
408 was confirmed by the KRM results (Table 4). The formation of J- and H-aggregates subpopulations in the
409 case of *b-4* dimers is difficult to identify by analyzing only the CD spectra; as such, changes of the
410 absorption spectra were also considered.

411 All dimer solutions exhibited fluorescence suppression relative to their monomer solutions. The
412 fluorescence suppression was reduced as $\log P_{o/w}$ decreased (increasing hydrophilicity) for non-chlorinated
413 and chlorinated dyes, except for transverse non-chlorinated dimers (Table 3 and SI 4). The emission
414 detected in the dimer solutions is likely caused by a small subpopulation of highly emissive SQ monomers
415 or “optical” monomers not forming an aggregate.¹⁴ The different fluorescence suppression between *b-2* and
416 *b-3* dimers reflects the effect of the SQ-DNA linker position in these SQs. The higher fluorescence
417 suppression exhibited by *b-2* (72 - 87%) than *b-3* (46 - 73%) is consistent with the A2/A1 ratio derived
418 from absorption spectra in these dimers. The effect on orientation and excitonic coupling strength by
419 changing the attachment positions of the dyes was confirmed with the KRM modeling (Section 3.4).

420 The aggregation tendencies of the SQs are consistent with the result of KRM modeling discussed
421 in Section 3.4. The photophysical changes of SQ dimers, such as blue-shifted absorption spectra relative to
422 the corresponding monomer, were influenced by the geometrical arrangement of SQ dimers and are
423 consistent with the characteristics of the type of aggregates described by Kasha based on the Frenkel exciton
424 theory¹ (Figure 1). The considerably quenched emission is consistent with enhanced nonradiative decay
425 upon SQs aggregation, and the residual emission may arise from a small subpopulation of “optical”
426 monomers.¹⁴

427



428
429
430

Figure 3. Experimental and modeled absorption and circular dichroism (CD) spectra of non-chlorinated squaraine dyes (plot in first and third rows). 3D plots of transition dipole moments of dyes (blue and red

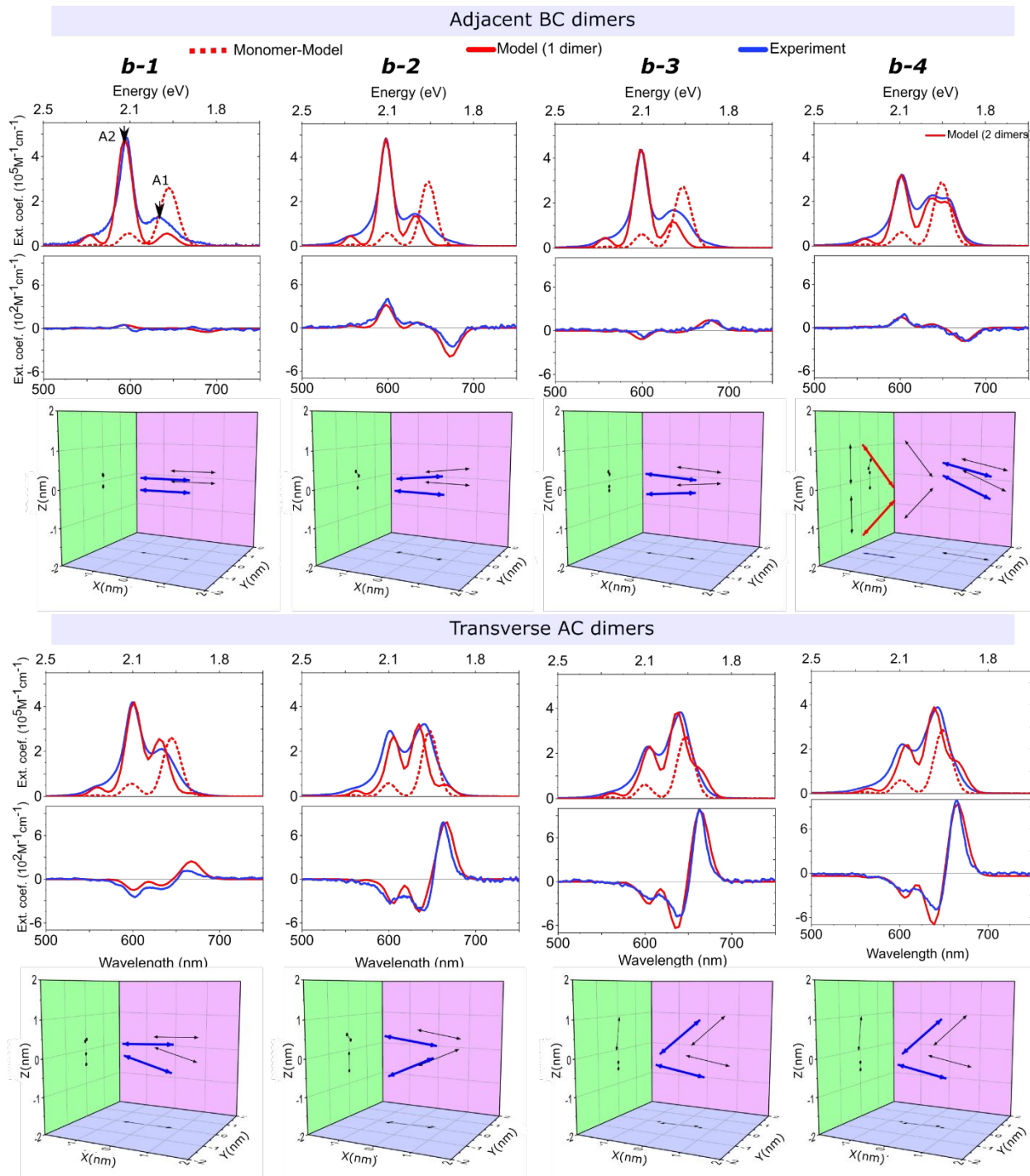
431 arrows projected to XY, YZ, and XZ planes in black arrows) derived from the KRM modeling (plots in
432 second and fourth rows). In heterogeneous aggregates, the distance between dimers is around 1 μ m.
433 Experimental data (absorption and CD) from our previous study³⁴ were used to refine the KRM modeling.
434 “A1” indicates the low energy absorbance peak aligned with the monomer spectra, and “A2” represents the
435 high energy absorbance peak that appears upon the formation of aggregates.

436

437 3.4. Geometry and Excitonic Delocalization of SQ dimers

438 The KRM modeling results showed that transverse *a-1*, *a-2*, *a-3*, and adjacent and transverse *b-1*
439 dimers likely form a single population of aggregates; $J_{m,n}$ and dimer orientations agrees with our previous
440 findings.³⁴ In contrast, adjacent dimers *a-1*, *a-2*, and *a-3* likely formed an ensemble-level mixture composed
441 of different subpopulations of aggregates, where one subpopulation of aggregate exhibited two-fold higher
442 $J_{m,n}$ with a shorter $R_{m,n}$ than the second subpopulation of aggregate (Table 4). Compared to the modeling
443 approach for a single population of aggregates (approach of homogeneous population of aggregates³⁴), the
444 modeling approach requiring multiple subpopulations (heterogeneous type of aggregates approach) of *a-1*,
445 *a-2*, and *a-3* dimers improved the goodness of fit between the modeled and experimental absorption and
446 CD spectra data (Figure 3).

447 The orientation estimated using the KRM modeling showed that most dimers have non-parallel
448 TDMs but still showed spectral features of H-aggregates (Figure 2 and 3). Since the range of estimated $J_{m,n}$
449 values (41 - 136 meV) for SQ aggregates is broad, SQ dimers were differentiated in two groups using the
450 median $J_{m,n}$ value of all SQ dimers investigated (66.5 meV). The group of dimers with $J_{m,n}$ smaller than the
451 median (66.5 meV) were mainly represented by transverse dimers ($R_{m,n} = 0.73 - 1.00$ nm and $\alpha_{m,n} = 34 -$
452 52°) and dimers with a lower $J_{m,n}$ of heterogeneous aggregates ($R_{m,n} = 0.62 - 1.46$ nm and $\alpha_{m,n} = 5 - 96^\circ$)
453 (Figure 5B-C). In contrast, the group of dimers with $J_{m,n}$ greater than the median value (66.5 meV) were
454 mainly represented by adjacent dimers and transverse *a-2* and *b-1* dimers that exhibited $R_{m,n}$ between 0.34
455 and 0.68 nm and $\alpha_{m,n}$ between 1 and 28° (Figure 5A).



456

457 Figure 4. Experimental and modeled absorption and circular dichroism (CD) spectra of the chlorinated
 458 squaraine dyes (plots in first and third rows). 3D plots of transition dipole moments of dyes (blue and red
 459 arrows projected to XY, YZ, and XZ planes in black arrows) derived from the KRM modeling (plot in
 460 second and fourth rows). In heterogeneous aggregates, the distance between dimers is around 1 μ m.
 461 Experimental data (absorption and CD) of *b-1* dimer was taken from our previous study.³⁴ “A1” indicates
 462 the low energy absorbance peak aligned with the monomer spectra, and “A2” represents the high energy
 463 absorbance peak that appears upon the formation of aggregates.

464 Table 4. Geometric parameters of squaraine dye dimers calculated using the theoretical approach of the
 465 Kühn–Renger–May model (KRM model)

Attachment in DNA-HJ	Dye Group	Dye Label	$J_{m,n}$ [meV]	$R_{m,n}$ [nm]	$d_{m,n}$ [nm]	$\alpha_{m,n}$ [°]	θ_m [°]	θ_n [°]	θ_t [°]	
Adjacent BC	Non-chlorinated	Control	a-1*	136	0.34	0.34	1	85	85	-1
				53	0.62	0.45	5	50	53	5
		Modified dyes	a-2*	47	0.70	0.65	4	78	76	3
			a-3*	117	0.39	0.36	4	85	83	-3
	Chlorinated	Control	b-1	48	0.87	0.37	41	43	85	-2
				109	0.44	0.42	2	88	86	-1
		Modified dyes	b-2	132	0.34	0.34	1	89	89	-1
			b-4*	100	0.42	0.34	10	90	83	-7
Transverse AC	Non-chlorinate	Control	a-1	103	0.46	0.34	10	84	86	3
				96	0.48	0.34	12	68	79	-6
		Modified dyes	b-3	-41	1.46	0.35	84	43	41	0
	Chlorinate	Control	a-2	50	1.00	0.36	50	66	63	1
			a-3	71	0.68	0.34	28	83	70	-5
		Modified dyes	b-1	62	0.91	0.35	44	67	69	2
			b-2	79	0.56	0.34	17	75	88	3
			b-4	62	0.73	0.34	34	66	82	9

$J_{m,n}$ is excitonic hopping parameter of dimers whose configuration is defined by the TDMs m and n . $R_{m,n}$ is the center-to-center dye distance. $d_{m,n}$ is the minimum distance between dyes; $\alpha_{m,n}$ is the angle between TDMs (supplementary if it is $>90^\circ$); θ_m and θ_n are the slip angles of TDMs m and n . θ_t is the twist angle of the TDMs m and n . Figure 2C represents the geometrical relations for $R_{m,n}$, $d_{m,n}$, θ_m , θ_n , and θ_t .

Star (*) indicates that these samples were modeled using the KRM model approach of two dimer subpopulations (multiple populations of dimers), which showed better fitting than the single dimer subpopulation approach.

The sign of $J_{m,n}$ does not influence the result of processing the Hamiltonian equation because it is related to the orientation of the corresponding transition dipole moment (TDM) vector.

466
 467 The attachment position of the dyes in the DNA-HJ was one of the important factors influencing
 468 $J_{m,n}$ between and geometry of dyes in aggregates of all samples. In agreement with previous studies,^{12,32–}
 469 ^{34,43} the present study demonstrated that the attachment position of SQs in the DNA-HJ impacts $J_{m,n}$ and
 470 geometry of dimers as follows. The adjacent dimers have $J_{m,n}$ greater than transverse dimers along with
 471 smaller $\alpha_{m,n}$ and $R_{m,n}$ (Table 4 and Figure 5A-C), highlighting that the proximity of dyes plays an essential
 472 role in the strength of excitonic interaction. This dye proximity can be influenced by the attachment point
 473 of the dye in the DNA. In the dye aggregates surveyed in the present study, large $R_{m,n}$ often results in large
 474 $\alpha_{m,n}$, with the latter dependent on the slip angles of each dye (θ_m and θ_n) and the twist angle (θ_t). The tendency
 475 for higher $J_{m,n}$ in adjacent dimers rather than transverse dimers may result from the physicochemical

476 interaction of dyes with DNA templates as demonstrated at single molecule level.³¹ Such interaction is
477 driven by the unique physicochemical environment where the dyes reside.⁶⁵ The observed effect of the SQs
478 position on the template is opposite to the one reported for substituted Cy5s⁴³, in which transverse dimers
479 exhibit a higher $J_{m,n}$ than adjacent dimers. The opposite $J_{m,n}$ results between SQs and Cy5s in adjacent and
480 transverse positions in DNA-HJ may be due to the different linkers. While Cy5s in the cited study were
481 attached to the DNA via two linkers that restrict the degrees of freedom, SQs in this study are attached to
482 the DNA via single flexible linker covalently bound to a modified thymine base. Such attachment condition
483 of SQs, in contrast to the Cy5s, may allow sufficient spatial freedom for the SQs to explore multiple dye
484 packing configurations and potentially find the optimal configuration.

485 The control *a-1* and *b-1* dimers exhibited higher $J_{m,n}$ than dyes modified with sulfo substituents.
486 Interestingly, the adjacent *b-1* dimers formed only one population of aggregates with $J_{m,n} = 132$ meV. In
487 contrast, the sample of adjacent *a-1* dimer formed a mixture of aggregates with $J_{m,n} = 136$ and 53 meV. The
488 KRM modeling approach of heterogeneous subpopulation of aggregates applied to *a-1* dimer showed an
489 improved fit over that of the single dimer approach reported in our previous study³⁴ (Figure 4, Section SI
490 5.1 and SI 6). Further studies are needed to elucidate the reasons leading to the formation of heterogenous
491 subpopulations of the dimer. The electron-withdrawing ability of *-Cl* in *b-1* dimer may intensify the
492 electrostatic attraction between indolenine rings of SQs and promote the formation of only one type of
493 dimer population.^{66,67}

494 The second important factor influencing $J_{m,n}$ between and geometry of dyes in aggregates of SQs is
495 the hydrophilicity quantified by $\log P_{o/w}$, which depends on the characteristics of substituents and their
496 location on the dye. The substituents of SQs in this work are characterized by different amounts of local
497 bulkiness and electron-withdrawing capabilities that have the potential to impact the molecular aggregation
498 in solution (Table 2). The amphiphilic behavior of *-buSl* substituent on the dye core may impact the
499 molecular packing. An asymmetric distribution of *buSl* substituents on the dye core may play an important

500 role, especially when changing the dye-DNA linker. Below is described the effect of hydrophilic
501 substituents of SQ dye for each non-chlorinated and chlorinated hydrophilic dyes.

502 The KRM modeling suggested that adjacent *a-2* and *a-3* dyes formed two dimer subpopulations,
503 one exhibiting stronger coupling than the other (Table 4). Compared to the single dimer approach,³⁴ the
504 heterogeneous subpopulation of aggregates approach improved the fitting between experimental and
505 modeled data of *a-2* and *a-3* dimers (Figure 4, Section SI 5.1 and SI 6). Solution of dimer *a-2* consisted of
506 subpopulations of aggregates with $J_{m,n} = 117$ and 47 meV. Solution of dimer *a-3* consisted of subpopulations
507 of aggregates with $J_{m,n} = 48$ and 109 meV, which is similar to solutions of dimer *a-1*. The presence of two
508 modeled subpopulations of aggregates in adjacent dimers but not in transverse dimers suggests that the
509 position of the dyes in the DNA-HJ may play a role in the formation of heterogeneous type of aggregate.
510 These results are consistent with observations of heterogeneity in aggregates of some adjacent dimers of
511 Cy5 and limited heterogeneity in aggregates of transverse dimers of Cy5.^{43,68} In most cases, heterogeneity
512 of Cy5 adjacent dimers resulted in dimer pairs with opposite chirality though with similar packing.⁴³
513 Interestingly, chirality of single population of SQ dimers can be controlled by using different lengths of dye
514 linkers.⁶⁹ The heterogeneity observed in adjacent dimers (*a-1*, *a-2*, *a-3*, and *b-4*) could result from two
515 major conformations (Iso I and Iso II)⁷⁰ that DNA-HJs may still adopt when SQs are attached. In samples
516 exhibiting heterogeneous aggregate populations, the dimer with high $J_{m,n}$ represents the maximum exciton
517 interaction strength that can be achieved with a given dye properties. Therefore, the highest $J_{m,n}$ of each
518 heterogeneous population was used to analyze the effect of dye hydrophilicity on exciton interaction
519 strength.

520 As expected and in agreement with our hypothesis, a linear regression analysis showed that
521 increased hydrophilicity reduces $J_{m,n}$ of adjacent dimers ($R^2 = 0.999$, Figure 5D-E). Likewise, as
522 hypothesized, larger $R_{m,n}$ was observed by increasing the SQs hydrophilicity. This result agrees with the
523 finding in Stadler *et al.*²⁸ It also provides updated insight on our observation in aggregates of SQs featuring
524 *Sl* and *buSl* substituents as reported in our previous study.³⁴ $J_{m,n}$ showed similar dependence on SASA (R^2

525 = 0.989) (Section SI 7) as hydrophilicity ($R^2 = 0.999$). However, for transverse dimers, there is no clear
526 trend between hydrophilicity and $J_{m,n}$ ($R^2 = 0.608$). Many studies have demonstrated that hydrophobic
527 interactions enhance dye aggregation^{28,71} because it promotes π - π stacking.^{72,73} Therefore, the modest
528 reduction of $J_{m,n}$ upon adding *buSl* substituents may be related to increased electrostatic and/or steric
529 repulsion of SQs. For example, electrostatic repulsion between sulfo substituents and/or steric repulsion of
530 sulfo butyl substituents may increase the intermolecular distance, reducing intermolecular interactions,
531 which decreases excitonic coupling as supported by the KRM modeling results for adjacent dimers. Hence,
532 the findings from the adjacent dimers of SQ dyes in this study support a general trend that increasing
533 hydrophilicity decreases $J_{m,n}$. Moreover, these results build upon and update the KRM modeling of SQ dyes
534 reported in our previous study.³⁴ The present study provides a mean of analysis of the structural
535 heterogeneity at the ensemble-level of these SQs. Further investigations are needed to elucidate the factors
536 influencing $J_{m,n}$ of non-chlorinated transverse dimers. It appears that hydrophilicity is not the main factor
537 governing dye aggregation.

538 According to the KRM modeling results, solutions of chlorinated SQ dimers consisted of a single
539 population of aggregate type, except for adjacent dimer *b-4*. Compared to the *-H* substituent of non-
540 chlorinated dyes, *-Cl* is a bulkier substituent (A-value = 0.47 kcal/mol) and has a weak electron-
541 withdrawing capacity ($\sigma_p = 0.23$). These two characteristics of *-Cl*, combined with neutral charge impart
542 hydrophobic properties to the dye, which might promote the formation of a single population of aggregate
543 type. Hydrophobic interactions enhance the π - π stacking as discussed above. Compared to adjacent
544 chlorinated dimers, transverse chlorinated dimers showed a lower $J_{m,n}$ with a higher θ_t (Table 4) that derives
545 from the high intensity of CD spectra depicted in Figure 4, indicating that the TDMs are not perfectly
546 parallel. Unlike transverse dimers, adjacent dimers *b-2* ($J_{m,n} = 100$ meV) and *b-3* ($J_{m,n} = 103$ meV) showed
547 similar excitonic interaction strengths. This result was expected because dyes *b-2* and *b-3* have the same
548 hydrophilic properties but different positions of the SQ-DNA linker. Surprisingly, transverse *b-2* ($J_{m,n} = 71$
549 meV) and *b-3* ($J_{m,n} = 62$ meV) dimers showed slightly different $J_{m,n}$; that may result from the combined

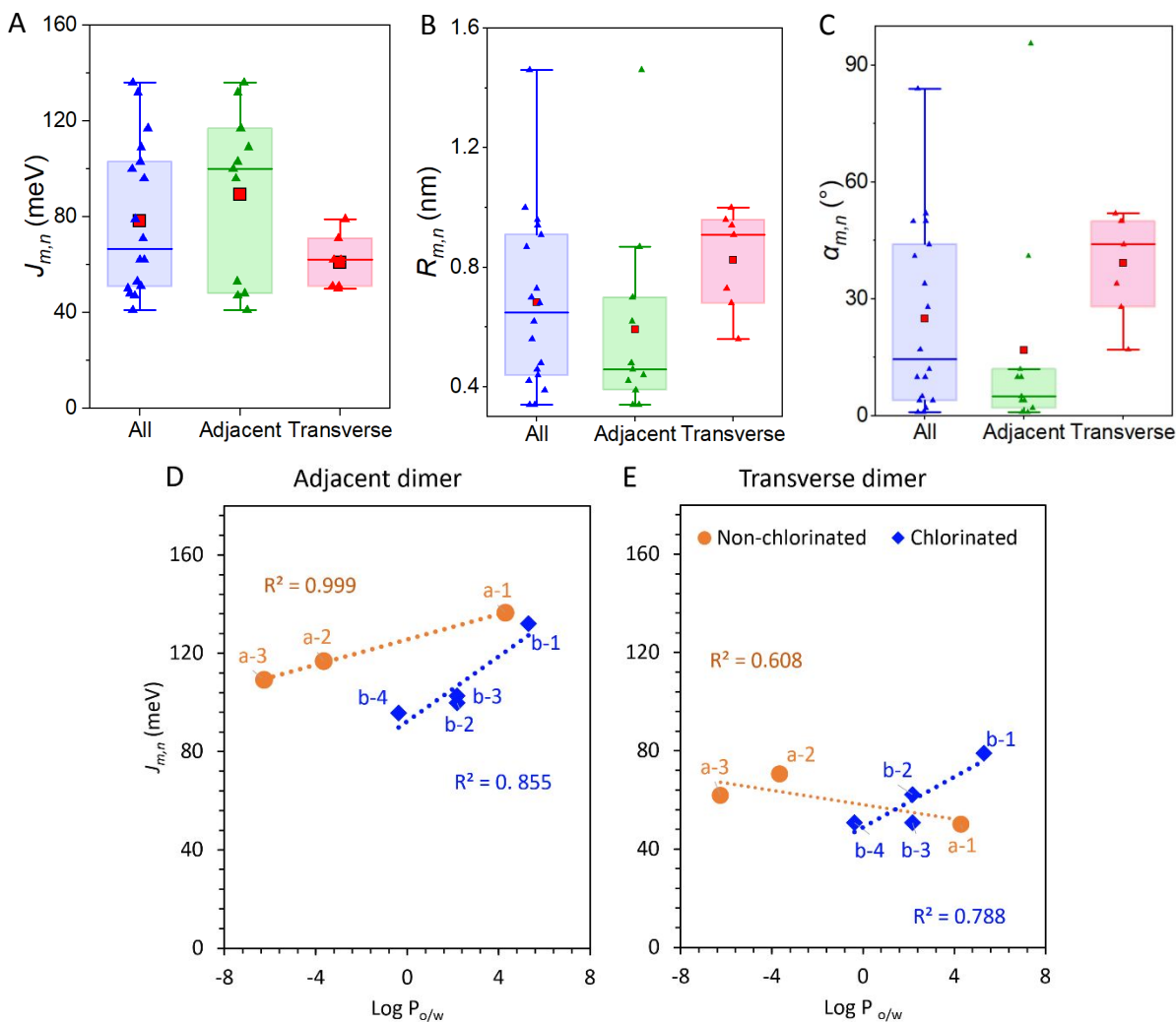
550 effect of the position of the SQ-DNA linker and SQs in the DNA-HJ. This result suggests that the
551 attachment positions of dyes in the DNA-HJ and in the SQ-DNA linker in the SQ could contribute to
552 changes in the molecular packing.

553 Interestingly, our modeling indicated that solutions of the adjacent dimer *b-4* consisted of a mixture
554 of two subpopulations of aggregates. The red-shifted and blue-shifted absorption spectra depicted by dimer
555 *b-4* relative to its monomer (Figure 4) prompted an intensive KRM modeling work using multiple
556 subpopulations to model the heterogeneous population at the ensemble-level. The results suggested that
557 dimer *b-4* forms population of aggregates with $J_{m,n} = 96$ meV that has a minimum intermolecular distance
558 ($d_{m,n}$) 0.34 nm, and another with $J_{m,n} = -41$ meV that has $d_{m,n} = 0.35$ nm. The mixture of aggregates
559 subpopulations might result from more hydrophilic behavior *b-4* due to the two hydrophilicity imparting
560 substituents *-buSl* as compared with *b-2* and *b-3* with a single *-buSl* (Table 2). Given the current limitation
561 of our KRM tool to tune the ratio of subpopulations of aggregates, the accurate estimation of the ratio of
562 aggregate types remains challenging. The estimation of dye orientations and aggregate types ratios within
563 a population would be possible in future studies using new approaches and methods of KRM modeling tool
564 that involves the combination of experiments and theory.

565 Increasing the dye hydrophilicity of chlorinated dyes via the presence of sulfo substituents led to a
566 larger $R_{m,n}$ and resulted in a smaller $J_{m,n}$. Using the maximum $J_{m,n}$ that was observed in *b-4*, the linear
567 regression analysis confirmed that hydrophilicity reduces excitonic interaction strength of adjacent ($R^2 =$
568 0.855) and transverse ($R^2 = 0.788$) dimers of chlorinated SQs (Figure 5D-E). $J_{m,n}$ of adjacent ($R^2 = 0.711$)
569 and transverse ($R^2 = 0.672$) dimers showed a lower dependency on SASA (Section SI 7). The latter result
570 agrees with the finding for non-chlorinated dyes that $\log P_{o/w}$ is a better predictor of $J_{m,n}$, as compared with
571 SASA. Results of chlorinated dimers reconfirm the hypothesis that hydrophilicity reduces $J_{m,n}$ because sulfo
572 substituents enhance the dye solubility and enlarge the intermolecular distance as discussed above. Findings
573 of Guckian *et al.*⁷² on aggregation of dyes non-covalently bound to DNA support that other factors such as

574 dipole moment, polarizability, and surface area are less important factors than hydrophobicity in stabilizing
 575 molecular packing.

576



577

578 Figure 5. (A) Excitonic hopping parameter ($J_{m,n}$), (B) center to center dye distance ($R_{m,n}$) and (C) angle
 579 between the transition dipole moments ($\alpha_{m,n}$) of squaraine dimers. In the boxplots, lower and upper values
 580 of the whiskers are the 5th and 75th percentiles; lower and upper extremes of the box are the 25th and 75th
 581 percentiles; line inside the box indicates the median value; and the red square (■) is the mean value of each
 582 data set. Relation between $J_{m,n}$ and hydrophobicity ($\log P_{o/w}$) of adjacent (D) and transverse (E) squaraine
 583 dimers.

584 Dimers with the symmetric distribution of substituents $-H$ ($a-1$; control), $-SI$ ($a-2$), and $-Cl$ ($b-1$)

585 were further analyzed to gain better insight into the effect of substituents on $J_{m,n}$. The $b-4$ dimer was not

586 included in this analysis to avoid bias due to the *-Cl* and *-buSl* substituents in each indolenine ring. The
587 substituents of SQs, with different local bulkiness (A-value) and electron-withdrawing capacity (Hammett
588 constant, σ), conferred a unique water affinity and SASA to SQs. The A-value of substituents increased as
589 SASA increased, though this relation does not indicate causation. That is because A-value indicates the
590 difference between the energies of equatorial and axial cyclohexane conformation resulting from the
591 presence of a substituents while SASA is the solvent accessible area of SQ. σ did not show a trend with
592 SASA or hydrophilicity. There was no clear trend of $J_{m,n}$ by increasing the hydrophilicity of the three
593 symmetrically substituted dyes. Interestingly, a negative relationship was observed between the A-value
594 and $J_{m,n}$ of adjacent dimers ($R^2 = 99.98\%$); in other words, $J_{m,n}$ decreased as the local bulkiness of the
595 substituents increased (Section SI 8). The unclear trend observed in transverse dimers ($R^2 = 19.1\%$) requires
596 further investigation to elucidate the factors affecting $J_{m,n}$. One possible explanation is the interaction of
597 dyes with neighboring bases. The result of adjacent dimers indicates that after the hydrophilicity of SQs,
598 A-value is a third factor potentially influencing $J_{m,n}$.

599 While results in the present study showed that the local bulkiness of substituents reduces $J_{m,n}$
600 between SQs in SQ dimers, a previous study found that bulkiness enhances $J_{m,n}$ between Cy5-R dyes in
601 Cy5-R dimers (R: substituents).⁴³ One possible reason for the opposite trend between SQs and Cy5-R
602 dimers when comparing $J_{m,n}$ and A-value could be due to the different water affinity of dye substituents.
603 The bulky tert-butyl substituent of Cy5-R⁴³ has hydrophobic properties that enhance π - π interactions while
604 the bulky *-Sl* substituent of SQs is hydrophilic which enhances the affinity of dyes to water and inhibits
605 molecular aggregation. This opposite physical property of substituents influences the behaviors of SQs in
606 solution and impacts their aggregation. Therefore, the influence of local bulkiness on the excitonic
607 interaction strength of Cy5-R and SQ dimers follow different trends. Overall, the dyes featuring hydrophilic
608 and amphiphilic substituents used in the present study exhibit high $J_{m,n}$ that can potentially be exploited for
609 developing molecular quantum materials given their solution processability.

610 4. Conclusions

611 This study demonstrated that non-chlorinated and chlorinated SQs with hydrophilic-imparting *-Sl*
612 and *-buSl* substituents readily form dimer aggregates when templated using DNA. These SQ dimer
613 aggregates showed different degrees of excitonic interaction strengths. One of the most important factors
614 determining the geometry and excitonic hopping parameter ($J_{m,n}$) is the attachment position of dyes in the
615 DNA-HJ. For example, all adjacent dimers showed higher $J_{m,n}$ than the transverse dimers. The second
616 important factor is the hydrophilicity of SQs ($\log P_{o/w}$), which increases by adding *-Sl* and *-buSl* substituents,
617 but also influenced by the presence of *-Cl* substituents. Therefore, the SQs were divided into non-
618 chlorinated and chlorinated groups and analyzed separately. Increased hydrophilicity of non-chlorinated
619 and chlorinated groups reduced $J_{m,n}$ because the *-Sl* and *buSl* substituents promoted the dye solubility in
620 water that enlarges the intermolecular distance hindering aggregation. The third important factor could be
621 the local bulkiness of the substituents. Additional factors such as SASA and electron-withdrawing capacity
622 appear to play less important roles in the packing of the molecular aggregates. However, further
623 investigation is needed to elucidate the factors influencing the $J_{m,n}$ of non-chlorinated transverse dimers.
624 Hence, the finding of the present study bridges to new exciting leading-edge technologies using dye with
625 hydrophilic-imparting substituents for developing molecular quantum materials.

626 The KRM tool was used to model heterogeneous populations formed by adjacent *a-1*, *a-2*, *a-3*, and
627 *b-4* dimers. The presence of multiple subpopulations formed by SQs suggested by the KRM modeling opens
628 research directions to further interrogate heterogeneous subpopulations using excitation-wavelength
629 dependent steady-state and time-resolved spectroscopies. Likewise, single molecule investigations could
630 allow the quantification of populations and their evolution over time. Reducing the heterogeneity of dye
631 aggregates while maintaining their strong excitonic interactions are challenges that need to be addressed to
632 improve control of exciton delocalization and application in quantum information systems.

633 Authors contribution

634 Investigation: GP and JL. Dye design: OAM, RDP, and JL. Dye synthesis: EAT, AT, OMO, and AIK.

635 Modeling of dye properties: GB and LL. Sample preparation and experiments: CKW and OAM. KRM code

636 developing and modeling: BY, SR, and GP. Data curation and formal analysis: GP, SR, and KC-S. Original

637 draft: GP and JL. Funding: JL, RDP, LL, OAM, and WBK. All authors: Writing – review and editing.

638 Authors Information

639 **Corresponding Author (*):**

640 **Jeunghoon Lee** – Micron School of Materials Science & Engineering and Department of Chemistry and

641 Biochemistry, Boise State University, Boise, Idaho 83725, United States. orcid.org/0000-0002-1909-4591.

642 Email: jeunghoonlee@boisestate.edu

643 **Authors**

644 **Gissela Pascual** – Micron School of Materials Science & Engineering, Boise State University, Boise, Idaho

645 83725, United States. orcid.org/0000-0002-7693-7815.

646 **Simon K. Roy** – Micron School of Materials Science & Engineering, Boise State University, Boise, Idaho

647 83725, United States, orcid.org/0000-0001-8652-1277

648 **German Barcenas** – Micron School of Materials Science & Engineering, Boise State University, Boise,

649 Idaho 83725, United States, orcid.org/0000-0002-9936-7720

650 **Christopher K. Wilson** – Micron School of Materials Science & Engineering, Boise State University,

651 Boise, Idaho 83725, United States; orcid.org/0000-0002-5197-6180

652 **Keitel Cervantes-Salguero** – Micron School of Materials Science & Engineering, Boise State University,

653 Boise, Idaho 83725, United States, orcid.org/0000-0001-8834-8711

654 **Olena M. Obukhova** – State Scientific Institution “Institute for Single Crystals” of the National Academy

655 of Sciences of Ukraine, Kharkiv 61072, Ukraine; orcid.org/0000-0002-5961-3202

656 **Alexander I. Krivoshey** – State Scientific Institution “Institute for Single Crystals” of the National
657 Academy of Sciences of Ukraine, Kharkiv, 61072, Ukraine; orcid.org/0000-0002-3820-5090

658 **Ewald. A. Terpetschnig** – SETA BioMedicals, LLC, Urbana, Illinois 61801, United States

659 **Anatoliy L. Tatarets**–State Scientific Institution “Institute for Single Crystals” of the National Academy
660 of Sciences of Ukraine, Kharkiv 61072, Ukraine; orcid.org/0000-0003-4406-7883

661 **Lan Li** – Micron School of Materials Science & Engineering, Boise State University, Boise, Idaho 83725,
662 United States; Center for Advanced Energy Studies, Idaho Falls, Idaho83401, United States

663 **Bernard Yurke** – Micron School of Materials Science & Engineering, Boise State University, Boise, Idaho
664 83725, United States; Department of Electrical & Computer Engineering, Boise State University, Boise,
665 Idaho 83725, United States; orcid.org/0000-0003-3913-2855

666 **William B. Knowlton** – Micron School of Materials Science & Engineering, Boise State University, Boise,
667 Idaho 83725, United States; Department of Electrical & Computer Engineering, Boise State University,
668 Boise, Idaho 83725, United States; orcid.org/0000-0003-3018-2207

669 **Olga A. Mass** – Micron School of Materials Science & Engineering, Boise State University, Boise, Idaho
670 83725, United States; orcid.org/0000-0002-2309-2644

671 **Ryan. D. Pensack**–Micron School of Materials Science & Engineering, Boise State University, Boise,
672 Idaho 83725, United States; orcid.org/0000-0002-1302-1770

673 Acknowledgment

674 The present research was supported wholly by the U.S. Department of Energy (DOE), Office of Basic
675 Energy Sciences, Materials Sciences and Engineering Division and DOE’s Established Program to
676 Stimulate Competitive Research (EPSCoR) program under Award DE-SC0020089.

677 Reference

- 678 1 M. Kasha, *Source: Radiation Research*, 1963, **20**, 55–70.
- 679 2 T. Mirkovic, E. E. Ostroumov, J. M. Anna, R. Van Grondelle, Govindjee and G. D. Scholes, *Chem*
680 *Rev*, 2017, **117**, 249–293.
- 681 3 F. Fassioli, R. Dinshaw, P. C. Arpin and G. D. Scholes, *J R Soc Interface*, 2014, **11**, 20130901.
- 682 4 B. Yurke, R. Elliott and A. Sup, *Phys Rev A*, 2023, **107**, 12603.
- 683 5 A. Huijser, P. L. Marek, T. J. Savenije, L. D. A. Siebbeles, T. Scherer, R. Hauschild, J.
684 Szymkowski, H. Kalt, H. Hahn and T. S. Balaban, *The Journal of Physical Chemistry C*, 2007, **111**,
685 11726–11733.
- 686 6 B. Yurke and W. Kuang, *Phys Rev A*, 2010, **81**, 033814.
- 687 7 C. Laboda, H. Duschl and C. L. Dwyer, *Acc Chem Res*, 2014, **47**, 1816–1824.
- 688 8 B. Yurke, in *Natural Computing Series*, eds. Janoska N. and Winfree E., Springer Science and
689 Business Media Deutschland GmbH, Singapore, 2023, vol. Part F821, pp. 125–169.
- 690 9 A. S. Klymchenko, *Acc Chem Res*, 2017, **50**, 366–375.
- 691 10 P. Zhang, M. S. Zhu, H. Luo, Q. Zhang, L. E. Guo, Z. Li and Y. B. Jiang, *Anal Chem*, 2017, **89**,
692 6210–6215.
- 693 11 D. Mathur, S. A. Díaz, N. Hildebrandt, R. D. Pensack, B. Yurke, A. Biaggne, L. Li, J. S. Melinger,
694 M. G. Ancona, W. B. Knowlton and I. L. Medintz, *Chem Soc Rev*, 2023, **52**, 7848–7948.
- 695 12 O. A. Mass, C. K. Wilson, S. K. Roy, M. S. Barclay, L. K. Patten, E. A. Terpetschnig, J. Lee, R. D.
696 Pensack, B. Yurke and W. B. Knowlton, *Journal of Physical Chemistry B*, 2020, **124**, 9636–9647.
- 697 13 N. J. Hestand and F. C. Spano, *Chem Rev*, 2018, **118**, 7069–7163.
- 698 14 J. S. Huff, P. H. Davis, A. Christy, D. L. Kellis, N. Kandadai, Z. S. D. Toa, G. D. Scholes, B. Yurke,
699 W. B. Knowlton and R. D. Pensack, *J Phys Chem Lett*, 2019, **10**, 2386–2392.
- 700 15 B. L. Cannon, D. L. Kellis, L. K. Patten, P. H. Davis, J. Lee, E. Graugnard, B. Yurke and W. B.
701 Knowlton, *J Phys Chem A*, 2017, **17**, 6905–6916.
- 702 16 U. Rösch, S. Yao, R. Wortmann and F. Würthner, *Angewandte Chemie - International Edition*,
703 2006, **45**, 7026–7030.
- 704 17 C. Zheng, C. Zhong, C. J. Collison and F. C. Spano, *The Journal of Physical Chemistry C*, 2019,
705 **123**, 3203–3215.
- 706 18 A. K. Singh, M. Fairoos, M. Kavungathodi, A. J. Mozer, K. Krishnamoorthy and J. Nithyanandhan,
707 *Langmuir*, 2022, **38**, 14808–14818.
- 708 19 W. J. Harrison, D. L. Mateer and G. J. T. Tiddy, *Journal of Physical Chemistry*, 1996, **100**, 2310–
709 2321.
- 710 20 I. G. Scheblykin, M. M. Bataiev, M. Van Der Auweraer and A. G. Vitukhnovsky, *Chem Phys Lett*,
711 2000, **316**, 37–44.

- 712 21 R. F. Khairutdinov and N. Serpone, *J. Phys. Chem*, 1995, **99**, 11952–11958.
- 713 22 Y.-C. Cheng and G. R. Fleming, *Annu Rev Phys Chem*, 2009, **60**, 241–262.
- 714 23 N. C. Seeman, *Nature*, 2003, **421**, 427–431.
- 715 24 B. Yurke, A. J. Turberfield, A. P. Mills J., F. C. Simmel and J. L. Neumann, *Nature*, 2000, **406**,
716 605–608.
- 717 25 N. C. Seeman, *Annu Rev Biochem*, 2010, **79**, 65–87.
- 718 26 V. L. Malinovskii, D. Wenger and R. Haner, *Chem Soc Rev*, 2010, **39**, 410–422.
- 719 27 A. L. Benveniste, Y. Creeger, G. W. Fisher, B. Ballou, A. S. Waggoner and B. A. Armitage, *J Am Chem*
720 *Soc*, 2007, **129**, 2025–2034.
- 721 28 A. L. Stadler, B. R. Renikuntla, D. Yaron, A. S. Fang and B. A. Armitage, *Langmuir*, 2011, **27**,
722 1472–1479.
- 723 29 R. A. Garoff, E. A. Litzinger, R. E. Connor, I. Fishman and B. A. Armitage, *Langmuir*, 2002, **18**,
724 6330–6337.
- 725 30 H. Asanuma, K. Shirasuka, T. Takarada, H. Kashida and M. Komiyama, *J Am Chem Soc*, 2003, **125**,
726 2217–2223.
- 727 31 K. Cervantes-Salguero, A. Biaggne, J. M. Youngsman, B. M. Ward, Y. C. Kim, L. Li, J. A. Hall,
728 W. B. Knowlton, E. Graugnard and W. Kuang, *Int J Mol Sci*, 2022, **23**, 7690.
- 729 32 B. L. Cannon, L. K. Patten, D. L. Kellis, P. H. Davis, J. Lee, E. Graugnard, B. Yurke and W. B.
730 Knowlton, *J Phys Chem A*, 2018, **122**, 2086–2095.
- 731 33 S. K. Roy, O. A. Mass, D. L. Kellis, C. K. Wilson, J. A. Hall, B. Yurke and W. B. Knowlton, *J Phys*
732 *Chem B*, 2021, **125**, 13670–13684.
- 733 34 O. A. Mass, C. K. Wilson, G. Barcenas, Ewald. A. Terpetschnig, O. M. Obukhova, O. S. Kolosova,
734 A. L. Tatarets, L. Li, B. Yurke, W. B. Knowlton, Ryan. D. Pensack and J. Lee, *The Journal of*
735 *Physical Chemistry C*, 2022, **126**, 3475–3488.
- 736 35 J. S. Huff, S. A. Díaz, M. S. Barclay, A. U. Chowdhury, M. Chiriboga, G. A. Ellis, D. Mathur, L.
737 K. Patten, S. K. Roy, A. Sup, A. Biaggne, B. S. Rolczynski, P. D. Cunningham, L. Li, J. Lee, P. H.
738 Davis, B. Yurke, W. B. Knowlton, I. L. Medintz, D. B. Turner, J. S. Melinger and R. D. Pensack,
739 *The Journal of Physical Chemistry C*, 2022, **126**, 17164–17175.
- 740 36 B. S. Rolczynski, S. A. Díaz, Y. C. Kim, I. L. Medintz, P. D. Cunningham and J. S. Melinger, *J*
741 *Phys Chem A*, 2021, **125**, 9632–9644.
- 742 37 M. Chiriboga, S. A. Diaz, D. Mathur, D. A. Hastman, J. S. Melinger, R. Veneziano and I. L. Medintz,
743 *J Phys Chem B*, 2022, **126**, 110–122.
- 744 38 M. I. Sorour, K. A. Kistler, A. H. Marcus and S. Matsika, *J Phys Chem A*, 2021, **125**, 7852–7866.
- 745 39 S. M. Hart, J. L. Banal, M. A. Castellanos, L. Markova, Y. Vyborna, J. Gorman, A. P. Willard, M.
746 Bathe and G. S. Schlau-Cohen, *Chem Sci*, 2022, **13**, 13020–13031.

- 747 40 S. M. Hart, W. J. Chen, J. L. Banal, R. Hä, M. Bathe, G. S. Schlau-Cohen, W. P. Bricker, A. Dodin,
748 L. Markova, Y. Vyborna and A. P. Willard, *Chem*, 2020, **7**, 752–773.
- 749 41 L. I. Markova, V. L. Malinovskii, L. D. Patsenker and R. Häner, *Org Biomol Chem*, 2012, **10**, 8944–
750 8947.
- 751 42 F. Nicoli, M. K. Roos, E. A. Hemmig, M. Di Antonio, R. De Vivie-Riedle and T. Liedl, *J Phys
752 Chem A*, 2016, **120**, 9941–9947.
- 753 43 S. A. Díaz, G. Pascual, L. K. Patten, S. K. Roy, A. Meares, M. Chiriboga, K. Susumu, W. B.
754 Knowlton, P. D. Cunningham, D. Mathur, B. Yurke, I. L. Medintz, J. Lee and J. S. Melinger,
755 *Nanoscale*, 2023, **15**, 3284–3299.
- 756 44 L. I. Markova, V. L. Malinovskii, L. D. Patsenker and R. Häner, *Chemical Communications*, 2013,
757 **49**, 5298–5300.
- 758 45 B. Ananda Rao, H. Kim and Y. A. Son, *Sens Actuators B Chem*, 2013, **188**, 847–856.
- 759 46 S. Sreejith, P. Carol, P. Chithra and A. Ajayaghosh, *J Mater Chem*, 2008, **18**, 264–274.
- 760 47 L. I. Markova, E. A. Terpetschnig and L. D. Patsenker, *Dyes and Pigments*, 2013, **99**, 561–570.
- 761 48 K. Iliina, W. M. Maccuaig, M. Laramie, J. N. Jeouty, L. R. McNally and M. Henary, *Bioconjug Chem*,
762 2020, **31**, 194–213.
- 763 49 L. Kringle, N. P. D. Sawaya, J. Widom, C. Adams, M. G. Raymer, A. Aspuru-Guzik and A. H.
764 Marcus, *J Chem Phys*, 2018, **148**, 85101.
- 765 50 O. Kühn, T. Renger and V. May, *Chem Phys*, 1996, **204**, 99–114.
- 766 51 N. M. Garrido, I. G. Economou, A. J. Queimada, M. Jorge and E. A. Macedo, *AIChE Journal*, 2012,
767 **58**, 1929–1938.
- 768 52 M. J. Frisch, H. B. Schlegel, G. E. Scuseria, M. A. Robb, J. R. Cheeseman, G. Scalmani, V. Barone,
769 F. G. A. Petersson, H. Nakatsuji, X. Li, M. Caricato, A. v Marenich, J. Bloino, B. G. Janesko, R.
770 Gomperts, B. Mennucci, H. P. Hratchian, J. v Ortiz, A. F. Izmaylov, J. L. Sonnenberg, D. Williams-
771 Young, F. Ding, F. Lipparini, F. Egidi, J. Goings, B. Peng, A. Petrone, T. Henderson, D. Ranasinghe,
772 V. G. Zakrzewski, J. Gao, N. Rega, G. Zheng, W. Liang, M. Hada, M. Ehara, K. Toyota, R. Fukuda,
773 J. Hasegawa, M. Ishida, T. Nakajima, Y. Honda, O. Kitao, H. Nakai, T. Vreven, K. Throssell, J. A.
774 Montgomery, J. E. Peralta, F. Ogliaro, M. J. Bearpark, J. J. Heyd, E. N. Brothers, K. N. Kudin, V.
775 N. Staroverov, T. A. Keith, R. Kobayashi, J. Normand, K. Raghavachari, A. P. Rendell, J. C. Burant,
776 S. S. Iyengar, J. Tomasi, M. Cossi, J. M. Millam, M. Klene, C. Adamo, R. Cammi, J. W. Ochterski,
777 R. L. Martin, K. Morokuma, O. Farkas, J. B. Foresman, D. J. Fox, G. W. Trucks, V. Fris Barone
778 and G. A. Petersson, *Gaussian16 Revision A.03*, 2016.
- 779 53 G. Barcenas, A. Biaggne, O. A. Mass, C. K. Wilson, O. M. Obukhova, O. S. Kolosova, A. L.
780 Tatarets, E. Terpetschnig, R. D. Pensack, J. Lee, W. B. Knowlton, B. Yurke and L. Li, *RSC Adv*,
781 2021, **11**, 19029–19040.
- 782 54 A. K. Rappe, C. J. Casewit, K. S. Colwell, W. A. Goddard and W. M. Skiff, *J. Am. Chem. Soc.*, 1992,
783 **114**, 10024–10035.

- 784 55 M. D. Hanwell, D. E. Curtis, D. C. Lonie, T. Vandermeersch, E. Zurek and G. R. Hutchison, *J*
785 *Cheminform*, 2012, **4**, 17.
- 786 56 Y. Zhao and D. G. Truhlar, *Theor Chem Acc*, 2008, **120**, 215–241.
- 787 57 T. D. Goddard, C. C. Huang, E. C. Meng, E. F. Pettersen, G. S. Couch, J. H. Morris and T. E. Ferrin,
788 *Protein Science*, 2018, **27**, 14–25.
- 789 58 N. M. O’Boyle, A. L. Tenderholt and K. M. Langner, *J Comput Chem*, 2008, **29**, 839–845.
- 790 59 E. Freytag, L. Kreimendahl, M. Holzapfel, J. Petersen, H. Lackinger, M. Stolte, F. Würthner, R.
791 Mitric and C. Lambert, *J Org Chem*, 2023, **88**, 10777–10788.
- 792 60 P. F. Santos, L. V. Reis, P. Almeida and D. E. Lynch, *CrystEngComm*, 2011, **13**, 1333–1338.
- 793 61 C. Hansch, A. Leo and R. W. Taft, *Chem. Rev*, 1991, **91**, 165–195.
- 794 62 H.-J. Schneider and V. Hoppen, *J Org Chem*, 1978, **43**, 3866–3873.
- 795 63 S. E. Boiadjev and D. A. Lightner, *J Am Chem Soc*, 2000, **122**, 11328–11339.
- 796 64 U. Mayerhöffer, M. Gsänger, M. Stolte, B. Fimmel and F. Würthner, *Chemistry - A European*
797 *Journal*, 2013, **19**, 218–232.
- 798 65 J. N. Wilson, J. Wiggenius, D. R. G. Pitter, Y. Qiu, M. Abrahamsson and F. Westerlund, *J Phys Chem*
799 *B*, 2013, **117**, 12000–12006.
- 800 66 M. Watt, L. K. E. Hardebeck, C. C. Kirkpatrick and M. Lewis, *J Am Chem Soc*, 2011, **133**, 3854–
801 3862.
- 802 67 E. G. Hohenstein, J. Duan and D. Sherrill, *J Am Chem Soc*, 2011, **133**, 13244–13247.
- 803 68 J. S. Huff, D. B. Turner, O. A. Mass, L. K. Patten, C. K. Wilson, S. K. Roy, M. S. Barclay, B. Yurke,
804 W. B. Knowlton, P. H. Davis and R. D. Pensack, *J Phys Chem B*, 2021, **125**, 10240–10259.
- 805 69 O. A. Mass, S. Basu, L. K. Patten, E. A. Terpetschnig, A. I. Krivoshey, A. L. Tatars, R. D. Pensack,
806 B. Yurke, W. B. Knowlton and J. Lee, *J. Phys. Chem. Lett*, 2022, **2022**, 10688–10696.
- 807 70 C. Hyeon, J. Lee, J. Yoon, S. Hohng and D. Thirumalai, *Nat Chem*, 2012, **4**, 907–914.
- 808 71 K. Umezawa, D. Citterio and K. Suzuki, *Analytical Sciences*, 2008, **24**, 213–217.
- 809 72 K. M. Guckian, B. A. Schweitzer, R. X-F Ren, C. J. Sheils, D. C. Tahmassebi and E. T. Kool, *J Am*
810 *Chem Soc*, 2000, **122**, 2213–2222.
- 811 73 K. M. Guckian, B. A. Schweitzer, R. X.-F. Ren, C. J. Sheils, P. L. Paris, D. C. Tahmassebi and E.
812 T. Kool, *J Am Chem Soc*, 1996, **118**, 8182–8183.

813

814